Draft version February 5, 2008
Preprint typeset using LaTeX style emulateapj v. 6/22/04

arXiv:astro-ph/0511594v1 19 Nov 2005

A SPECTROSCOPIC STUDY OF THE ENVIRONMENTS OF GRAVITATIONAL LENS GALAXIES

Ivelina Momcheva and Kurtis Williams
Steward Observatory, 933 N. Cherry Ave., Tucson, AZ 85721

Charles Keeton
Department of Physics and Astronomy, Rutgers University, Piscataway, NJ 08854

and

Ann Zabludoff
Steward Obs., 933 N. Cherry Ave., Tucson, AZ 85721

Draft version February 5, 2008

ABSTRACT

We present the first results from our spectroscopic survey[1] of the environments of strong gravitational lenses. The lens galaxy belongs to a poor group of galaxies in six of the eight systems in our sample. We discover three new groups associated with the lens galaxies of BRI 0952−0115 (five members), MG 1654+1346 (seven members), and B2114+022 (five members). We more than double the number of members for another three previously known groups around the lenses MG 0751+2716 (13 total members), PG 1115+080 (13 total members), and B1422+231 (16 total members). We determine the kinematics of the six groups, including their mean velocities, velocity dispersions, and projected spatial centroids. For the newly discovered groups, we quantify these properties for the first time. For the other three groups, the increased membership allows us to make more robust estimates of the kinematic properties of the groups than previously possible. The velocity dispersions of the groups range from 110^{+170}_{-80} to 470^{+100}_{-90} km s^{-1}. The higher velocity dispersions (for the richer groups MG0751, PG1115, and B1422) are consistent with those of nearby X-ray luminous groups, while the others (for the poorer groups BRI0952, MG1654, and B2114) are more typical of nearby dynamically younger groups. The lens galaxy is the brightest member in fewer than half of the groups. In general, the brightest group galaxy is an early-type galaxy that lies off the center of the potential and occupies an orbit indistinguishable from the other group members. In at least three of the lenses — MG0751, PG1115, and B1422 — the group environment significantly affects the lens potential. These lenses happen to be the quadruply-imaged ones in our sample, which suggests a connection between image configuration and environment. Finally, our survey allows us to assess for the first time whether mass structures along the line of sight are important for lensing. We first show that, in principle, the lens potential may be affected by line-of-sight structures over a wide range of spatial and redshift offsets from the lens. We then quantify real line-of-sight effects using our survey and find that at least four of the eight lens fields have substantial interloping structures close in projection to the lens, and at least one of those structures (in the field of MG0751) significantly affects the lens potential.

Subject headings: gravitational lensing — (galaxies:) quasars: individual (MG 0751+2716, BRI 0952−0115, PG 1115+080, B1422+231, MG 1654+1346, PMN J2004−1349, B2114+022, HE 2149−2745) — galaxies: clusters: general — galaxies: halos

1. INTRODUCTION

The study of strong gravitational lens systems offers critical constraints on the masses, shapes, evolution, and substructure of galaxy dark matter halos (e.g., Kochanek 1991; Keeton et al. 1998; Metcalf & Madau 2001; Dalal & Kochanek 2002; Rusin et al. 2003; Rusin & Kochanek 2005; Treu & Koopmans 2004; Ferreras et al. 2005), on the Hubble constant independent of the local distance ladder (e.g., Refsdal 1964; Kochanek & Schechter 2003), and on the dark energy density (e.g., Turner 1990; Kochanek 1996a; Chae 2003; Linder 2004; Mitchell et al. 2005). However, our understanding of observed lenses is limited by uncertainties and biases in the lens models necessary to analyze the data. Despite improving data for lensed images and lens galaxies, astrophysical applications of lensing are still hindered by poor knowledge of the environments in which strong lens systems reside.

Several arguments suggest that lenses have complex environments. Statistical arguments based on galaxy demographics imply that at least 25% of lens galaxies lie in dense environments such as groups and clusters (Keeton et al. 2000). From spectroscopic observations, several lenses are in fact known to lie in groups (MG 0751+2716, PG 1115+080, B1422+231, and B1608+656; Tonry & Kochanek 1999; Kundić et al. 1997a,b; Tonry 1998; Fassnacht et al. 2004), and several others in clusters (RX J0911+0551, Q0957+561, HST 14113+5221, and MG 2016+112; Kneib et al. 2000; Young et al. 1981b; Fischer et al. 1998; Soucail et al. 2001). Indirect evidence for the existence of other groups comes from the large tidal shears required to explain the image configurations of many four-image (quad) lenses,

[1]This paper includes data gathered with the 6.5 meter Magellan Telescopes located at Las Campanas Observatory, Chile.

which presumably come from mass structures near the lens galaxy or along the line of sight (Keeton et al. 1997). The range of required shears in quad lenses could reflect a range of environment densities, running from poor groups to rich clusters. Comparisons of the lensing rate in different surveys have also been cited as evidence that many lens galaxies probably lie in groups (Blandford et al. 2001). Finally, theoretical models predict that lens galaxies reside in complex environments that produce substantial shears, although it is not yet clear whether the models predict shears large enough to explain real quad lenses (Holder & Schechter 2003; Dalal & Watson 2004).

If not handled properly, complex environments can inject uncertainties and biases into the astrophysical quantities derived from lens models (see Keeton & Zabludoff 2004, hereafter KZ04). For example, neglecting environment altogether leads to lens models that, for most purposes,[1] are simply wrong. Approximating environmental effects with a simple shear term leads to models that are better but still tend to overestimate the Hubble constant, the velocity dispersion of the lens galaxy, and the dark energy density Ω_Λ, and to underestimate the magnifications of the lensed images. In principle, modeling the full richness of environmental effects can remove these biases, and may also resolve the long-standing puzzle of why quad lenses are almost as common as doubles in statistically complete lens samples (see King et al. 1996; Kochanek 1996b; Keeton et al. 1997; Rusin & Tegmark 2001; Cohn & Kochanek 2004, KZ04). Such an analysis requires detailed knowledge of the galaxy populations, velocity dispersions, and projected spatial centroids of groups and clusters around lenses in order to determine how the environments affect the lens potentials. To date, such observations have mainly been carried out for the few lenses that reside in clusters, which leaves many lenses whose environments are known poorly or not at all. Worse, existing observations cannot characterize the *distribution* of lens environments, so we cannot assess environment-related biases in statistical quantities (such as Ω_Λ or the quad/double ratio) or ensemble properties (such as evolution or substructure). While the environment distribution can be predicted from theoretical models (Keeton et al. 1997; Holder & Schechter 2003; Dalal & Watson 2004), disagreements among the models, and discrepancies between the predicted distributions and the shears required to fit observed lenses, raise questions about the predictions.

These issues have not been adequately addressed with observations, because no systematic survey of lens environments exists. Surveys of a few lens fields have been published individually or in pairs (Young et al. 1981b; Kundić et al. 1997a,b; Fischer et al. 1998; Tonry 1998; Tonry & Kochanek 1999; Kneib et al. 2000; Fassnacht & Lubin 2002; Fassnacht et al. 2004; Soucail et al. 2001). In many cases, though, those surveys only spanned a $\sim 30''$ field around each lens, so they did not adequately sample group or cluster membership out to the virial radius (~ 0.7 Mpc for groups, corresponding to $\sim 3'$ at the redshifts of the lenses we study). We have undertaken a systematic deep and wide-field survey of lens fields, and here we present results for the first eight systems that we have targeted for multi-object spectroscopy. We characterize the environment within a $\sim 6'$ diameter field around each of the eight lenses, and quantify how those environments affect the lens potentials.

Going beyond the lenses' immediate environments, we also consider the degree to which massive structures along the line of sight to a lens affect the lens potential. The prevalence and importance of interloping structures in lens fields is poorly understood. Observationally, there appear to be bound groups along the lines of sight to B0712+472 (10 members; Fassnacht & Lubin 2002) and MG 1131+0456 (3 members; Tonry & Kochanek 2000). Overdensities of galaxies are seen in the fields of several other strong lenses (Faure et al. 2004; Morgan et al. 2005), but it is not yet known whether they indicate massive bound structures, and whether any such structures are associated with the lens galaxies or lie elsewhere along the lines of sight. On the theoretical side, studies have yielded conflicting results as to whether line-of-sight structures are very important or negligible for lensing (e.g., Seljak 1994; Bar-Kana 1996; Keeton et al. 1997; Premadi & Martel 2004). We show here that lenses are, in principle, sensitive to structures over a wide range of redshifts and projected spatial offsets, so the practical importance of interloping structures depends only on how common they are. Our photometric/spectroscopic pencil-beam survey of lens fields enables us to self-consistently identify any prominent structures at all relevant redshifts, and to assess their actual contributions to observed lenses.

Separate from lensing, an important by-product of our survey is a sizable sample of poor groups at intermediate redshifts. Only a few such samples are presently known (Carlberg et al. 2001; Wilman et al. 2005; Gerke et al. 2005). Groups are important laboratories for studies of galaxy evolution because they are the most common environments for galaxies, and are also relatively simple systems in which the range of mechanisms thought to drive galaxy evolution (primarily galaxy–galaxy interactions) is much narrower than in hotter, denser clusters (Zabludoff & Mulchaey 1998a, hereafter ZM98). Unfortunately, poor groups are notoriously difficult to identify using conventional methods for finding clusters, due to their low projected surface densities, faint X-ray luminosities, and inefficiency for weak lensing. The velocity dispersions of nearby groups range from $\sigma_r \sim 200$ km s^{-1} for systems that are X-ray faint, late-type dominated, dynamically young, and generally similar to the Local Group; to $\sigma_r \sim 300$–500 km s^{-1} for systems that are richer, X-ray luminous, early-type dominated, and dynamically more evolved; up to $\sigma_r \sim 1000$ km s^{-1} for rich clusters. In nearby X-ray luminous groups with $\sigma_r \sim 300$–500 km s^{-1}, there is always a giant elliptical that lies at the center of the group potential, which suggests that such galaxies form in groups via interactions prior to being accreted by rich clusters (ZM98). Groups at intermediate redshifts like those we describe here will, in conjunction with nearby group samples, permit us to observe the evolution of groups directly.

The organization of this paper is as follows. In §2 we

[1] The important exception is measurements of the total mass within the Einstein radius, which are largely independent of assumptions built into lens models (e.g., Kochanek 1991; Cohn et al. 2001).

describe our sample of eight lens systems and summarize previous work on them. In §3 we present our spectroscopic data in the eight lens fields. In §4 we determine the membership, kinematics, and centroids of the groups, and use those properties to quantify how the environments affect the lens models. We also explore the effects of line-of-sight structures on the lens models. We summarize our results and conclusions in §5. We present the formalism for computing the convergence and shear arising from perturbing structures anywhere along the line of sight in an Appendix. Where necessary, we assume a cosmology with $\Omega_M = 0.3$, $\Omega_\Lambda = 0.7$, and $H_0 = 70$ km s^{-1} Mpc^{-1}.

2. THE SAMPLE

Our sample consists of eight known gravitational lens systems with lens galaxies at intermediate redshifts $0.25 < z_l < 0.5$. Four of the lenses (MG 0751+2716, PG 1115+080, B1422+231, and MG 1654+1346) were suspected from previous studies to have complex environments. We chose the other four lenses (BRI 0952−0115, PMN J2004−1349, B2114+022, and HE 2149−2745) because of the availability of prior imaging and photometry as well as accessibility from Las Campanas Observatory. In the remainder of this section we briefly review prior studies of these eight lenses. The data from this section are summarized in Table 1.

MG 0751+2716 (hereafter MG0751), discovered as a part of the MIT–Greenbank–VLA search for gravitational lenses, is a radio lens with four images and a partial ring (Lehár et al. 1993). Optical imaging of the system by Lehár et al. (1997) identified an $R = 21.3$ galaxy (G3) located $0.2''$ northeast of the brightest radio spot as the likely lens galaxy. G3 is a satellite of a much brighter $R = 19.1$ galaxy (G1) located $6''$ away. Tonry & Kochanek (1999) determined the redshifts of the galaxies to be $z_{G1} = 0.3501 \pm 0.0003$ and $z_{G3} = 0.3502 \pm 0.0003$. They also found a nearby emission line galaxy to have redshift 0.3505 ± 0.0003, indicating that the lens galaxy lies in a small group with at least three members. Lens models by Lehár et al. (1997) suggest that MG0751 requires more external shear that can be accounted for by the observed galaxies, which is consistent with the hypothesis that the lens environment is complex. The redshift of the source quasar is $z_s = 3.200 \pm 0.001$ (Tonry & Kochanek 1999).

BRI 0952−0115 (hereafter BRI0952) was discovered by McMahon & Irwin (1992) as a doubly imaged $z_s = 4.5$ optical quasar. The quasar is also detected at millimeter wavelengths (Omont et al. 1996). Keeton et al. (1998) found that the lens is a flattened early type galaxy, and Kochanek et al. (2000) estimated a lens redshift of $z_l = 0.41 \pm 0.05$ based on fundamental plane fitting. Because the separation between the images is small ($0.9''$) and the lens galaxy is faint (21.9 in F675W; Keeton et al. 1998), the lens redshift has not been determined spectroscopically.

PG 1115+080 (hereafter PG1115) is a lens system discovered by Weymann et al. (1980), in which a radio-quiet quasar at redshift $z_s = 1.722$ is lensed into four images (Hege et al. 1981). The lens galaxy was first detected by Henry & Heasley (1986); its redshift was estimated by Angonin-Willaime et al. (1993), and later improved by Kundić et al. (1997a) and Tonry (1998) to $z_l = 0.3098 \pm 0.0002$. Young et al. (1981a) suggested the presence of a small group of galaxies near the lens. This was confirmed by Kundić et al. (1997a) and Tonry (1998), who measured the redshifts of a total of four galaxies within $20''$ of the lens galaxy. Kundić et al. (1997a) estimated a group velocity dispersion of $\sigma_r = 270 \pm 70$ km s^{-1} from four galaxies, while Tonry (1998) estimated $\sigma_r = 326$ km s^{-1} from a slightly different set of four galaxies. Grant et al. (2004) detected diffuse X-ray emission that is associated with the group and that has a temperature $kT \sim 0.8 \pm 0.2$ keV; this value is consistent with typical values for low-redshift poor groups, but somewhat high given the measured group velocity dispersion and the local σ_r-T_X relation (Mulchaey & Zabludoff 1998, hereafter MZ98). PG1115 is one of nine known strong lens systems for which the time delay between different images has been measured, so it can be used to determine H_0. Schechter et al. (1997) measured the light curves of the different images and estimated the time delays, and Bar-Kana (1997) then reanalyzed the data to give more precise results: the delay between images B and C is $t_{BC} = 25.0^{+3.3}_{-3.8}$ days, and the ratio of the delays between A (actually a combination of the close images A_1 and A_2), B, and C is $t_{AC}/t_{BA} = 1.13^{+0.18}_{-0.17}$. PG1115 is one of the lenses with "anomalous" flux ratios thought to indicate some sort of small-scale structure in the lens galaxy (e.g., Metcalf & Madau 2001; Chiba 2002; Dalal & Kochanek 2002; Keeton et al. 2005a).

B1422+231 (hereafter B1422) is a four-image lens discovered by Patnaik et al. (1992) while searching for small-separation lenses among flat spectrum radio sources in the Jodrell Bank–VLA Astrometric Survey (JVAS; Patnaik et al. 1992a; Browne et al. 1998; Wilkinson et al. 1998; King et al. 1999). The source is a radio loud quasar at $z_s = 3.62$ (Patnaik et al. 1992), and the lens is a luminous elliptical at $z_l = 0.3374$ (Impey et al. 1996; Kundić et al. 1997b). The lens galaxy and five nearby galaxies form a group at $z_g = 0.338$ with a rest-frame line-of-sight velocity dispersion of $\sigma_r = 550 \pm 50$ km s^{-1} (Kundić et al. 1997b). Lens models for B1422 require a significant shear $\gamma \sim 0.20$–0.26, which may be attributable to the group environment (Hogg & Blandford 1994; Keeton et al. 1997; Dobler & Keeton 2005). Indeed, from their estimate of the group's velocity dispersion and centroid, Kundić et al. (1997b) estimated $\gamma = 0.23$ and pointed out that the group will also create some convergence κ that may affect the lens potential. Grant et al. (2004) detected B1422 in X-rays (0.5–2 keV) and determined a temperature of $kT = 1.0^{+\infty}_{-0.3}$ keV, which is consistent with the value expected for a poor group (MZ98). B1422 is another lens with "anomalous" flux ratios (Mao & Schneider 1998; Chiba 2002).

MG 1654+1346 (hereafter MG1654) was originally detected in the MIT–Greenbank–VLA survey. Langston et al. (1988, 1989) recognized its unusual structure in a VLA snapshot and obtained radio and optical mapping. The source is a $z_s = 1.74$ radio quasar with a compact core and two extended radio lobes. The southwest lobe is lensed into a ring by a $z_l = 0.254$ giant elliptical galaxy (Langston et al. 1988; Kochanek et al. 2000). Langston et al. (1989) noted an enhancement of the number density of galaxies near the lens; some of the

TABLE 1
Gravitational Lens Galaxies

Lens	RA[b] (J2000)	Dec[b] (J2000)	z_l	I[b] [mag]	z_s[b]	Δt[e] [days]	Images[b, f]	kT_X[e] [keV]	$N_{\rm grp}$[d, e]	σ_r[e] [km s^{-1}]
MG 0751+2716	07:51:41.46	+27:16:31.4	0.349[a]	21.26	3.20	-	R	-	2	-
BRI 0952−0115	09:55:00.01	−01:30:05.0	(0.41)[c]	21.21	4.50	-	2	-	-	-
PG 1115+080	11:18:17.00	+07:45:57.7	0.31[b]	18.92	1.72	25.0±2.0	4	0.8±0.2	4	270±70
B1422+231	14:24:38.09	+22:56:00.6	0.34[b]	19.66	3.62	-	4	$1.0^{+\,\inf}_{-0.3}$	5	550±50
MG 1654+1346	16:54:41.83	+13:46:22.0	0.254[a]	17.9	1.74	-	R	-	-	-
PMN J2004−1349	20:04:07.07	−13:49:30.7	-	-	-	-	2	-	-	-
B2114+022	21:16:50.75	+02:25:46.9	0.316[a] 0.59[b]	18.63	-	-	2+2	-	-	-
HE 2149−2745	21:52:07.44	−27:31:50.2	0.50[b]	19.56	2.03	103.0±12.0	2	-	-	-

[a]Data from this work
[b]Data from references in the text and from the CASTLES website (`http://cfa-www.harvard.edu/castles/`).
[c]Photometric redshift (Kochanek et al. 2000)
[d]Number of previously known group members in addition to the lens galaxy.
[e]References in text.
[f]R means an Einstein ring.

nearby galaxies are comparable in brightness to the lens galaxy, suggesting a complex environment.

PMN J2004−1349 (hereafter PMN2004) is a two-image lens discovered in a search for radio lenses in the southern sky (Winn et al. 2001). The radio spectral index of the images is typical for radio-loud quasars, so the source is considered to be a quasar despite the lack of an optical spectrum and a measured redshift (Winn et al. 2001). Based on photometry, Winn et al. (2001) suggested a lens redshift in the range $0.5 < z_l < 1.0$. Higher-resolution imaging by Winn, Hall & Schechter (2003) revealed a spiral lens galaxy (only the fifth one known) and showed that the color differences between the two images at optical and near-infrared wavelengths can be explained by differential extinction. The extinction analysis can be used to infer the lens redshift; it seems to imply somewhat low values ($0.03 \lesssim z_l \lesssim 0.36$), but that result depends on assumptions about the extinction curve.

B2114+022 (hereafter B2114) was discovered as part of the search for lenses in JVAS (King et al. 1999). Radio maps show four distinct components within 2.4″ in a configuration that is atypical for lenses. Furthermore, the sources can be divided into two pairs with distinct radio surface brightnesses and radio spectra: sources A and D are similar to each other, and sources B and C are similar to one another, but the two pairs are clearly different. Ground-based and HST optical imaging and spectroscopy do not detect the lensed images but reveal two lens galaxies at $z_{l1} = 0.3157$ and $z_{l2} = 0.5883$ (Augusto et al. 2001), suggesting a complex lensing geometry. Chae, Mao & Augusto (2001) could explain two of the radio components (A and D) as lensed images using a two-plane lens model. It is not known whether the other components (B and C) are images of the same source (unlikely), images of a different source, or structure related to the G1 lens galaxy. No lens models that explain these components have been published.

HE 2149−2745 (hereafter HE2149) is a doubly imaged broad absorption line quasar at redshift $z_s = 2.033$, which was discovered by Wisotzki et al. (1996) in the Hamburg/ESO wide-angle survey for bright quasars. Burud et al. (2002) reported a redshift of $z_l = 0.495 \pm 0.01$ for the elliptical lens galaxy, consistent with the photometric redshift estimate of $z_l = 0.43^{+0.07}_{-0.06}$ (Kochanek et al. 2000). Burud et al. also measured the time delay between the two images to be $\Delta t = 103 \pm 12$ days. Based on the large number of red non-stellar objects in R-band images of the field around the lens, Lopez, Wucknitz & Wisotzki (1998) suggested that the lens galaxy might be a member of a cluster.

3. SPECTROSCOPIC DATA

We first identified galaxies for follow-up spectroscopy from two-color, wide-field imaging of each lens field. We obtained deep images in I and either V or R during the period from May 2002 to June 2004 using the $36' \times 36'$ Mosaic Imager on the 4-m telescopes at Kitt Peak National Observatory and Cerro Tololo Inter-American Observatory. We reduced these images and extracted photometric catalogs following standard methods using IRAF[2] and SExtractor (Bertin & Arnouts 1996). A more detailed description of the photometric analysis is presented in a separate paper (Williams et al. 2005).

We selected spectroscopy targets using a prioritization scheme based on objects' colors and projected distances from the lens. Highest priority was given to objects populating a red sequence in the color–magnitude diagram that is consistent with the lens redshift, and to targets that lie within a group-like virial radius of 0.7 Mpc (ZM98), which corresponds to $\sim 3'$ over the redshift range of our lenses. We applied a magnitude cut at $I = 21.5$ to assure reasonable exposure times. This limiting magnitude corresponds to $I^* + 4.2$ at the low redshift limit of our sample ($z = 0.25$) and to $I^* + 2.8$ at the high redshift limit ($z = 0.5$), where I^* is the observed magnitude of an L_* galaxy, adopted from Williams et al. (2005). We obtained multislit spectroscopy during two observing runs, March 1–4 and August 30–September

[2] IRAF is distributed by the National Optical Astronomy Observatories, which are operated by the Association of Universities for Research in Astronomy, Inc., under cooperative agreement with the National Science Foundation.

2, 2003, with the Low Dispersion Survey Spectrograph (LDSS-2; Allington-Smith et al. 1990) at the 6.5-m Magellan 2 (Clay) telescope at Las Campanas Observatory. All spectra were taken with the medium blue grism (300 l/mm; 5000Å blaze) over a wavelength range of 3900–8000Å. We used 1.03″ slitlets, resulting in a spectral resolution of ≈ 15Å FWHM. Each slitmask had dimensions $\sim 5' \times 7'$, typically contained 20–30 targets, and was observed for 4×900 s.

Our sky coverage is shown in Figure 1. Each panel spans $15' \times 15'$ and is centered on the lens galaxy. Rectangles show the outlines of our slitmasks. There is a noticeable difference in the sampling between the two observing runs. In March 2003, when we observed MG0751, BRI0952, PG1115, B1422, and MG1654, the masks lay mostly on top of one another, providing exhaustive coverage of the immediate surroundings of each lens galaxy. Because most of our fields were far north for Magellan, we aligned the masks with the paralactic angle to minimize the effects of atmospheric dispersion. In contrast, the masks for MG1654, PMN2004, B2114, and HE2149 in the August 2003 observing run were tiled to cover a larger area of the sky but still overlap significantly in the 3′ projected radius around the lens. No attempt was made to align the masks with the paralactic angle because the targets were close to or south of the celestial equator and were therefore observed at relatively low airmass.

The figure shows that our sampling is very good within 3′ around the lens for all fields, with a minor exception in B1422. We observed four masks for each of MG0751, BRI0952, PG1115 and B1422, five masks for each of PMN2004, B2114 and HE2149, and seven masks for MG1654 (which was observed during both runs). We discuss our spectroscopic completeness below.

We reduced all spectra using standard IRAF procedures and corrected them to the local standard of rest using the IRAF routines RVCORRECT and DOPCOR. We determined the radial velocities using the cross-correlation of absorption lines (XCSAO) and/or using emission line identifications (EMSAO)[3]. If both emission and absorption line velocities were found, the quoted value is a weighted average of the two. Marc Postman kindly provided template galaxy spectra (Postman et al. 2002, and private communications). We visually inspected every fit to ensure accuracy.

The number of objects observed in each field is listed in Table 2. Galaxies represent ∼42% of the objects targeted spectroscopically, while stars originally misclassified as galaxies are ∼22%. "Failed" targets (∼ 32%) are those for which were unable to obtain velocities. The majority of failed targets, especially at fainter magnitudes, were absorption-line systems for which the signal-to-noise was too low to allow successful cross-correlation. Other causes of failures are low surface brightness or poor astrometry (more problematic in March than August). The fraction of stars was significantly lower in August (15%) than in March (26%), thanks to improvements in star-galaxy separation made between the two runs (see Williams et al. 2005). The large number of stars in PMN2004 is due to the high stellar density at this relatively low galactic latitude and longitude ($l = 28°$, $b = -22°$).

Figure 2 shows the completeness of our spectroscopy with respect to the photometry. The solid-line histogram shows the magnitude distribution for all galaxies in the photometric catalog projected within 3′ of the lens, while the shaded histogram shows the subset for which we determined velocities. Our target selection scheme, based on colors and projected offsets from the lens, misses a few of the brightest galaxies (many of which are likely to be foreground objects). We miss a larger fraction of objects at the faint end, but these are very few and/or less massive galaxies, which would significantly affect the lens potential only if very close to the lens galaxy. In total, there are only four galaxies within 10″ of the lens galaxies (the zone in which a small perturber can have even a moderate effect; see Fig. 6 below) that are present in our photometric catalog but have no determined velocities. Two of those (in B2114 and PMN2004) are below our spectroscopic magnitude limit of $I = 21.5$. The other two galaxies are in the field of HE2149, have I magnitudes of 19.97 and 21.08, and lie 7″ and 10″ respectively from the lens. In color–magnitude space (Williams et al. 2005) they lie on red sequences identified as line-of-sight structures at $z = 0.45$ and $z = 0.60$ (see §4.5).

We were never able to put slits on all of our highest-priority objects; this limitation is inherent to multislit spectroscopy. For lensing purposes, the main effect of spectroscopic incompleteness is to cause us to *underestimate* environment-related lensing biases (see §§4.4–4.5). In particular, the fact that we prioritize galaxies thought to lie at the lens redshift (color selection) means that we undersample line-of-sight structures and hence underestimate their contributions to the lens potential.

As already mentioned, we improved our photometric catalogs after some of the spectroscopic targets were selected. As a result, there are 15 galaxies whose velocities we measured that do not actually appear in the final photometric catalog. (These galaxies lie under bleed trails in the imaging, so accurate photometry is not possible.) In addition, there are another 25 galaxies whose velocities we measured that are (mis-)classified in the final photometric catalog as stars. We omit all of these galaxies when comparing the spectroscopic and photometric catalogs for the purpose of understanding our spectroscopic completeness (i.e., they are excluded from Fig. 2). However, these remain a part of our spectroscopic catalog and all analyses based on that catalog.

To estimate the zero-point velocity correction and external velocity errors, we cross-correlate 403 sky spectra extracted from our data with the same templates used for the galaxy spectra and find a mean velocity of $\bar{v} = 40 \pm 50$ km s^{-1}. We also determine the velocities of 153 of the serendipitously observed stars and find $\bar{v} = 30 \pm 180$ km s^{-1}. Both methods give mean velocities comparable to or smaller than the dispersion, and much smaller than the velocities of the objects in the sample. We therefore conclude that no zero point correction is needed.

Table 3 lists our spectroscopic catalog. For each entry we give the catalog name, J2000 coordinates calibrated to USNO-B2.0, projected distance from the lens in arcmin, aperture magnitude within a fixed physical size of ∼6.5 kpc (see Williams et al. 2005), the heliocentric radial velocity, velocity error, redshift and redshift error.

[3] XCSAO and EMSAO are routines in the RVSAO IRAF package (Kurtz & Mink 1998)

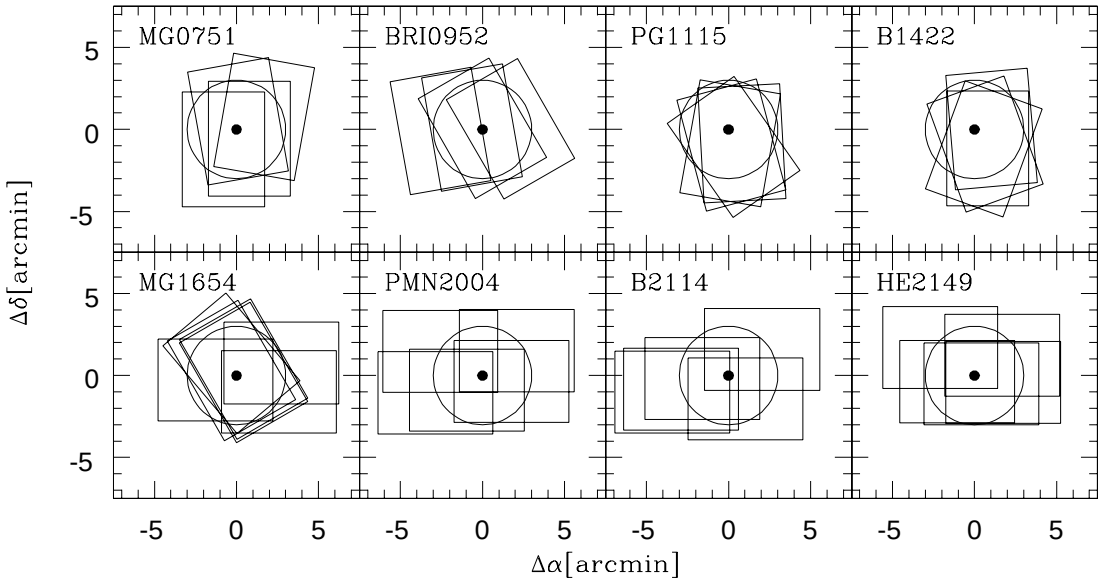

FIG. 1.— Sky coverage for LDSS-2 multislit spectroscopy in the fields of the eight lens systems in our sample. Each panel is $15' \times 15'$, centered on the lens galaxy. Rectangles show the positions of our slit masks. Each slitmask covers $\sim 5' \times 7'$ and includes 20–30 slitlets parallel to the long side of the mask. The $3'$ circle around the lens galaxy corresponds to ~ 0.7 Mpc, a group-like virial at the redshifs of the lenses in our sample. We observed four masks for each of MG0751, BRI0952, PG1115, and B1422, five masks for each of PMN2004, B2114, and HE2149, and seven masks for MG1654. The masks from the first observing run lack a particular sampling pattern but provide excellent coverage of the expected group virial radius in all cases except B1422, where a small portion remains unsampled. The masks from the second observing run were tiled in an attempt to maximize the sky coverage while still providing good sampling of the immediate surroundings of the lens.

TABLE 2
LDSS-2 OBSERVATIONS

Lens	Date	# Galaxies[a]	# Stars	# Failed	Total
MG0751	March 2003	38	24	27	89
BRI0952	March 2003	47	24	19	90
PG1115	March 2003	47	28	11	86
B1422	March 2003	53	14	26	93
MG1654	March 2003	39	30	32	101
	August 2003	20	6	35	61
PMN2004	August 2003	41	43	35	119
B2114	August 2003	38	1	46	85
HE2149	August 2003	41	8	66	115

[a]Including QSOs.

The last column describes the method from which the velocity was obtained: 1 for absorption lines, 2 for emission lines, or 3 for a combination of both. Missing data means that the object was not in the final photometric catalog as described above. Such objects have no identification names and are numbered successively starting with 90001.

4. RESULTS AND DISCUSSION

4.1. *Group Membership*

The environments of most strong lenses are not well characterized. Our first goal is to determine whether each lens galaxy lies in a group or cluster, and if so to identify the other member galaxies. Even in cases where groups were already identified (MG0751, PG1115, and B1422), the number of group members known previously ranged from three to six. Our deep, wide-field spectroscopic sampling has the potential not only to find new groups, but also to increase the membership of known lens groups to the point where robust determinations of the group velocity dispersions and centroids are possible. These are essential for understanding how a group affects the lens potential, as discussed in §4.4. Additionally, a more complete inventory of the brightest (most massive) group members, and their contributions to the lens potential, will also greatly improve lens models.

We present the redshift histograms for all eight of our lens fields in Figure 3. In the left panels, the shaded histograms include all galaxies that lie within a projected radius of $3'$ (a group-like virial radius) around the lens, and

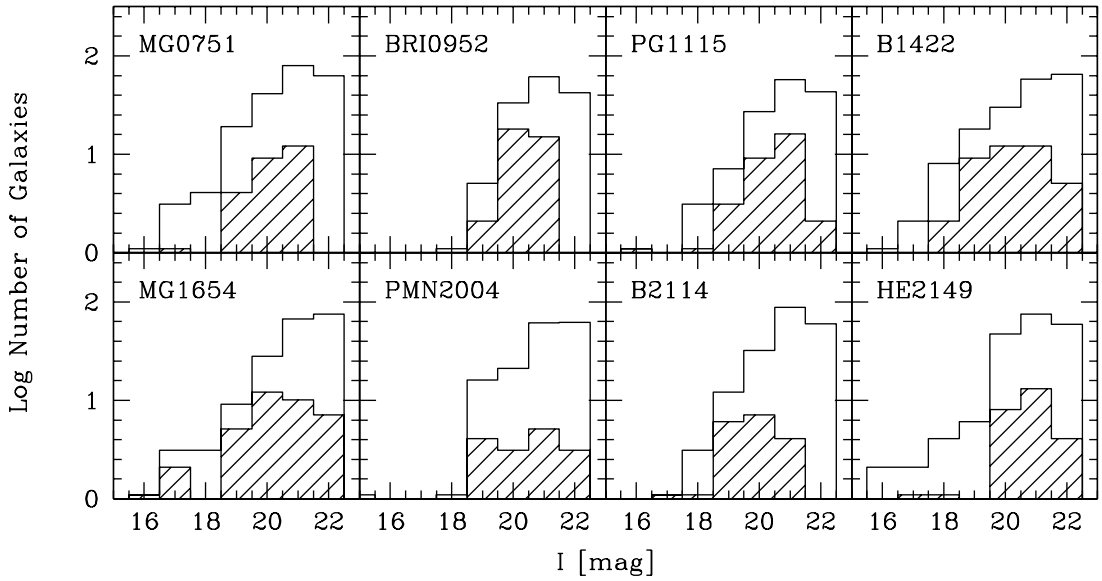

FIG. 2.— Apparent magnitude histograms of galaxies in the photometric catalog (*solid line*), and of those galaxies within 3′ of the lens for which redshifts were obtained (*shaded*). Our target selection scheme, based on colors and projected offsets from the lens, misses a few of the brightest galaxies. We miss a larger fraction of objects at the faint end, but these are presumably less massive galaxies that do not contribute significantly to the lens potential.

TABLE 3
LENS FIELD GALAXY PROPERTIES — EXAMPLE

ID	α [hh:mm:ss]	δ [dd:mm:ss]	b [']	I [mag]	cz [km s^{-1}]	Δcz	z	Δz	Spectral Type
MG0751: MWKZ GAL									
... 9809	07:51:30.20	27:14:43.1	3.10	20.9	168070	30	0.56023	0.000083	2
... 9739	07:51:30.77	27:17:55.7	2.76	20.6	105970	70	0.35323	0.000237	2
... 9726	07:51:31.00	27:14:16.7	3.24	20.5	175630	50	0.58543	0.000173	3
... 9582	07:51:32.04	27:12:59.2	3.30	19.0	91080	30	0.30360	0.000113	3
... 9606	07:51:32.28	27:12:58.9	4.10	20.8	106950	100	0.35650	0.000320	1
... 9570	07:51:32.49	27:17:38.6	2.29	20.2	104680	30	0.34893	0.000113	3
... 9560	07:51:32.73	27:14:42.1	2.67	21.0	106300	30	0.35433	0.000113	2
... 9333	07:51:34.61	27:15:45.5	1.71	19.5	91220	50	0.30407	0.000153	1
... 9297	07:51:34.66	27:13:37.7	3.28	18.4	28910	40	0.09637	0.000133	1
... 9274	07:51:35.24	27:17:37.1	1.76	19.6	105350	110	0.35117	0.000380	1
... 9225	07:51:35.43	27:17:07.9	1.48	19.0	79820	60	0.26607	0.000213	3
... 9239	07:51:35.75	27:15:22.8	1.72	20.9	104960	80	0.34987	0.000280	1
... 9100	07:51:36.66	27:19:39.8	3.31	18.4	74510	50	0.24837	0.000160	1
... 9047	07:51:36.96	27:19:27.9	3.10	18.3	104220	40	0.34740	0.000140	2
... 9120	07:51:36.98	27:18:40.6	2.37	20.9	72100	60	0.24033	0.000203	2
... 9049	07:51:37.73	27:18:06.5	1.78	20.4	71940	50	0.23980	0.000163	2
... 8794	07:51:37.92	27:16:12.9	0.85	0.0	167590	100	0.55863	0.000320	1
... 9006	07:51:38.04	27:17:33.7	1.28	20.1	168620	90	0.56207	0.000307	1
... 8816	07:51:40.32	27:16:22.1	0.31	20.9	104940	100	0.34980	0.000323	1
... 8669	07:51:41.07	27:19:43.7	3.20	18.9	147320	120	0.49107	0.000390	1
... 8682	07:51:41.50	27:16:31.9	0.00	20.1	104810	120	0.34937	0.000410	1
... 8673	07:51:41.84	27:16:29.2	0.09	21.5	167090	10	0.55697	0.000037	2
... 8476	07:51:43.25	27:17:53.3	1.41	19.8	169470	210	0.56490	0.000687	1
... 7921	07:51:43.26	27:16:06.3	0.58	0.0	124780	30	0.41593	0.000103	3
... 8385	07:51:44.18	27:16:39.7	0.61	20.7	112430	200	0.37477	0.000657	1
... 8257	07:51:45.32	27:17:02.4	0.99	19.4	105110	60	0.35037	0.000200	1
... 8288	07:51:45.50	27:18:51.4	2.49	20.4	60380	100	0.20127	0.000317	1

NOTE. — This table is published in its entirety in the electronic edition. A portion is shown here for guidance regarding its form and content. Objects with missing data were not found in our final photometric catalog for reasons explained in the text.

$N_{\rm tot}$ indicates the number of galaxies in the histogram. This number excludes a few high-redshift AGNs that fall outside the range of the plot. The histograms include all galaxies with spectroscopic redshifts both from our sample and from the literature. In particular, we have added the following 16 galaxies to our catalog: G1, G6, and G7 in MG0751 (Tonry & Kochanek 1999); the lens galaxy GL as well as Gx in PG1115 (Tonry 1998); the lens galaxy G1 as well as G2, G3, G4, G6, G8, G9, G10, and Gx in B1422 (Kundić et al. 1997b; Tonry 1998); the $z_l = 0.59$ lens galaxy in B2114 (Augusto et al. 2001); and the $z_l = 0.495 \pm 0.01$ lens galaxy in HE2149 (Burud et al. 2002). We have not included the lens galaxy in BRI0952 (because it only has a photometric redshift estimate) or in PMN2004 (because no good redshift estimate exists). The vertical line shows the position of the lens galaxy as listed in Table 1. In six cases (see Table 4), there is clearly a peak in redshift space at or near the lens galaxy redshift.

We determine the group membership by applying a pessimistic 3σ clipping algorithm (as suggested by Yahil & Vidal 1977) to any redshift peak containing a lens galaxy. This procedure removes the galaxy most deviant from the mean redshift and recalculates the mean and velocity dispersion of the distribution. If the omitted galaxy is more than three new standard deviations away from the recomputed mean, it is rejected. This loop is executed until an omitted galaxy is not rejected. We use statistical bi-weight estimators, which are more robust for small sample sizes than the standard estimators (Beers et al. 1990), to calculate the location (mean redshift) and scale (velocity dispersion). In Figure 3, $N_{\rm grp}$ is the number of group members determined by the 3σ clipping algorithm.

The right-hand panels in Figure 3 show a cut within ± 5000 km s^{-1} of the lens galaxy velocity to present a better view of the lens groups themselves. The peak height is lower than in the full histogram because the bin size is smaller, but groups are still easily recognizable in six cases: MG0751, BRI0952, PG1115, B1422, MG1654 and B2114. *The groups in BRI0952, MG1654, and B2114 are new discoveries. For the previously known groups, we have increased the number of group members from three to 13 in MG0751, from five to 13 in PG1115, and from six to 16 in B1422.* The projected spatial distributions of galaxies in the six groups are shown in Figure 4.

In the case of BRI0952, we suggest that the lens galaxy may belong to the five-member group at $z_g = 0.422$, which is consistent with its photometric redshift estimate of $z_l = 0.41 \pm 0.05$. In B1422, the group seems to consist of two clumps — one around the lens galaxy and the other to the northeast of it (see Figure 4). Zabludoff & Mulchaey (1998b) have found analogous substructure in nearby groups. B1422 is our best sampled group (16 members) and we expect that increasing the membership of the other groups might reveal similar clumpiness. In B2114, the group is associated with the foreground lens galaxy (the first vertical dashed line). There is a second peak slightly in front of the group around the lens galaxy, but the galaxies are significantly offset from the lens on the sky and thus not important for lensing. We classify as "group members" only the galaxies in the peak at the lens redshift.

Our spectroscopic findings agree well with the expectations set by our photometry (see Williams et al. 2005). All six lenses where we find groups show a compelling red sequence at the lens redshift. In HE2149, the color–magnitude diagram shows a well defined red sequence corresponding to $z \sim 0.28$, where we see a prominent line-of-sight structure in Figure 3. In PMN2004, the lack of compelling structures in either the color–magnitude diagram or the redshift histogram suggests that there are no significant structures along the line of sight, although it is difficult to draw firm conclusions from non-detections (especially given incomplete spectroscopy). In any case, the agreement between our photometric and spectroscopic results reassures us that we understand the data and their implications. These results are discussed further in Williams et al. (2005).

4.2. *Group Kinematics*

The group velocity dispersion provides a key observable probe of the group potential and its effect on lens models. Group velocity dispersions based on small member catalogs are uncertain and may be biased, because poor sampling of the underlying velocity distribution tends to underestimate the true velocity dispersion (ZM98). Our more extensive member catalogs now allow us to measure the group velocity dispersions more accurately than was previously possible.

To determine the mean velocities, $\bar{v}$, and line-of-sight velocity dispersions, σ_r, of the six groups in our sample, we use bi-weight estimators of location and scale (Beers et al. 1990) because of their superiority at deweighting tails in the velocity distribution. In BRI0952, which has only five members, the bi-weight estimator routine fails, so we use the standard method for calculating the mean velocity and velocity dispersion from Danese et al. (1980). In general, standard and bi-weight methods yield similar means and velocity dispersions. We use all known group members, including the 10 found in the literature, to determine these kinematic properties. We apply a standard $1/(1+z_g)$ cosmological correction to the velocity dispersions (Beers et al. 1990). The kinematic properties of the groups are presented in Table 4.

The six groups have velocity dispersions ranging from 110^{+170}_{-80} to 470^{+100}_{-90} km s^{-1}. In the nearby universe, this range of velocity dispersions describes systems running from dynamically young, unrelaxed systems like the Local Group, up to more dynamically relaxed, X-ray luminous groups. We are probably seeing a similar range of groups in our intermediate-redshift sample. It is important to note that the total number of galaxies for which velocities were obtained is similar in all six fields, and that $N_{\rm grp}$ is roughly correlated with σ_r, suggesting that the differences between the measured σ_r values are real and not due to variable sampling.

As a further check on the accuracy of our group velocity dispersions, we can determine the X-ray temperature that would be derived by combining our measured σ_r values with the σ_r-T_X relation for nearby groups and clusters (ZM98), and compare that with the temperature measured directly from X-ray observations. Only two of the groups in our sample have been observed in X-rays with *Chandra*: PG1115 and B1422 (Grant et al. 2004). The X-ray temperatures expected from the σ_r-T_X relation (1.5 keV and 1.7 keV, respectively) are consistent

TABLE 4
Group Kinematic Properties

Lens	$N_{\rm tot}$	$N_{\rm grp}$	α_{cen}	$\sigma_{\alpha,cen}$ [″]	δ_{cen}	$\sigma_{\delta,cen}$ [″]	v_{min} [$km\,s^{-1}$]	v_{max}	$\bar{v}$ [$km\,s^{-1}$]	$\delta\bar{v}$	z	$\sigma_{r,\rm grp}$ [$km\,s^{-1}$]	$\delta\sigma_{r,\rm grp}$
MG0751	39	13	07:51:40.7	±11	+27:16:53	±9	104220	105970	104980	±100	0.3499	320	$^{+170}_{-110}$
BRI0952	44	5	09:54:56.1	±34	−01:29:58	±27	125000	127000	126510	±30	0.4217	170[a]	$^{+150}_{-100}$
PG1115	48	13	11:18:16.8	±11	+07:45:36	±9	92120	93960	92970	±110	0.3090	440	$^{+90}_{-80}$
B1422	57	16	14:24:41.0	±11	+22:55:42	±9	100640	102810	101540	±130	0.3385	470	$^{+100}_{-90}$
MG1654	59	7	16:54:39.3	±27	+13:47:15	±20	75390	76210	75750	±100	0.2525	200	$^{+120}_{-80}$
B2114	38	5	21:16:51.4	±34	+02:10:59	±27	93000	95000	94240	±80	0.3141	110	$^{+170}_{-80}$

[a]Velocity dispersion calculated in the manner of Danese et al. (1980), instead of using the statistical bi-weight estimator of scale (Beers et al. 1990). See text.

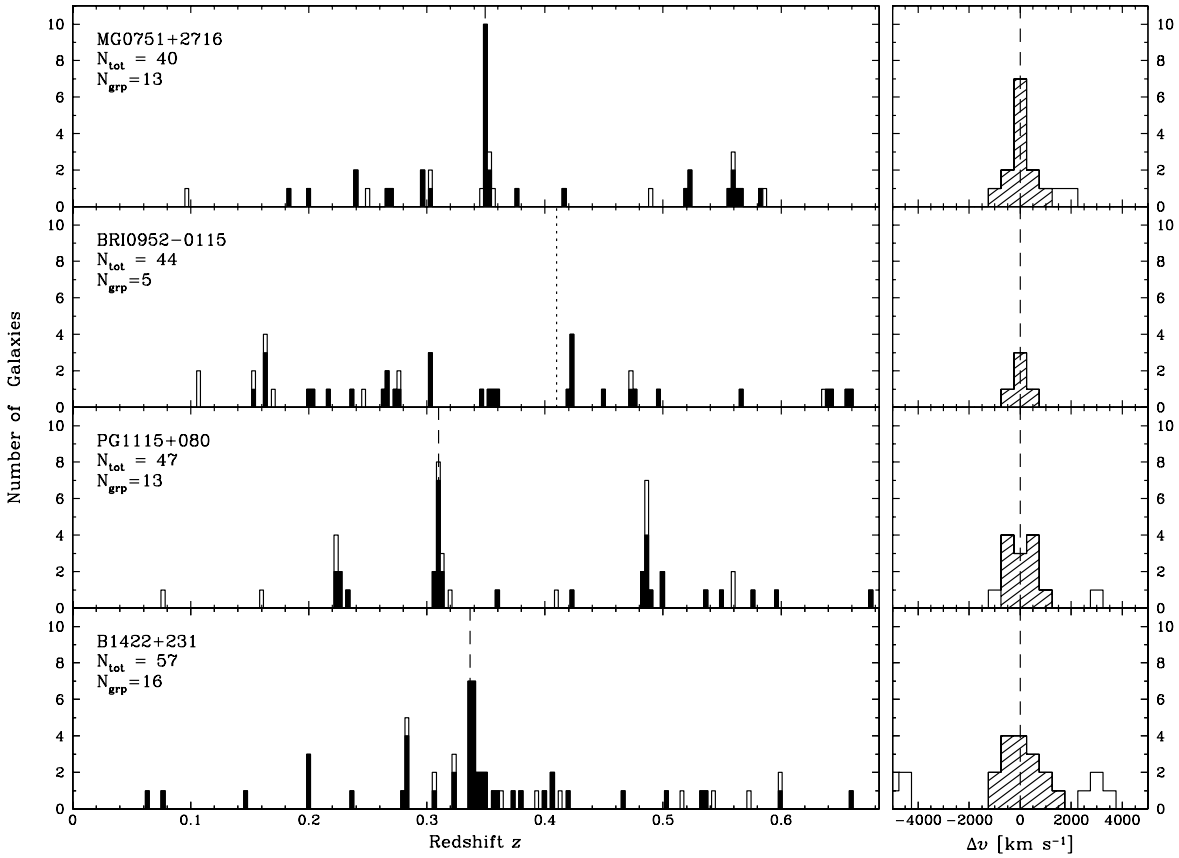

Fig. 3.— *(Left)* Galaxy redshift distributions of the eight fields in our sample. The bin size is 1000 km s^{-1}. The shaded histogram includes all galaxies that lie within a projected radius of 3′ about the lens. The vertical dashed lines show spectroscopic lens galaxy redshifts from the literature. The vertical dotted line for BRI0952 shows a photometric estimate of the lens galaxy redshift. In PMN2004, the vertical dot-dashed lines show two different model-implied estimates of the lens galaxy redshift (Winn, Hall & Schechter 2003). $N_{\rm tot}$ is the total number of galaxies included in the histogram, while $N_{\rm grp}$ is the total number of group members. *(Right)* A close-up of the range ±5000 km s^{-1} centered on the mean group velocity. The bin size is 500 km s^{-1}. The shaded histogram shows confirmed group members.

within the 95% confidence limit with the observed values (0.8 keV and 1.0 keV, respectively). This suggests that our values of σ_r for these groups are reasonable.

4.3. *Group Centroids*

The projected offset of the lens galaxy from the group centroid is another key ingredient in estimating the contribution of a group to the lens potential. The position of the brightest group galaxy relative to the spatial and kinematic centroid of the group is also an important con-

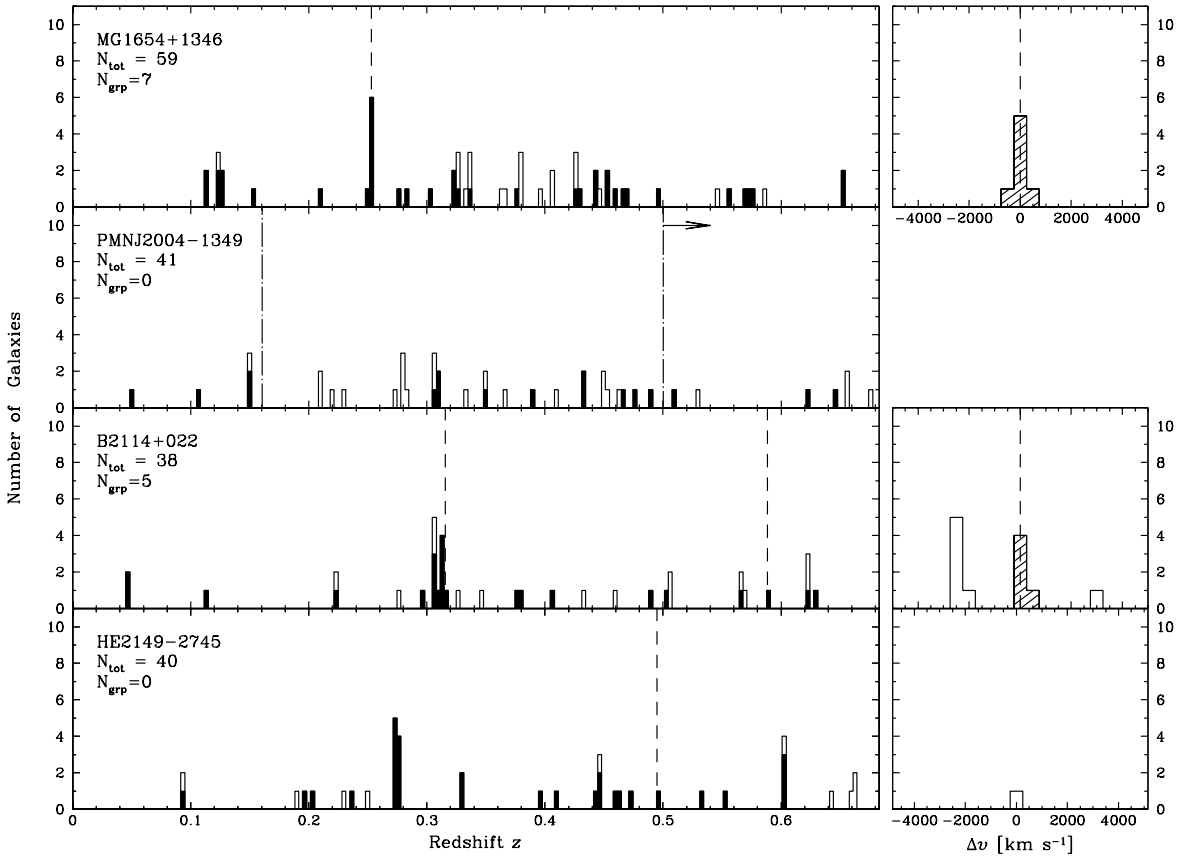

FIG. 3.— continued.

straint on models of giant elliptical formation (ZM98). (The lens galaxy may or may not be the brightest group galaxy, as discussed below.) In this section we calculate the projected spatial and kinematic centroids of the groups by averaging the sky positions and velocities, respectively, of all group members. For members whose velocities were added from the literature, we use coordinates from our own photometric catalog when possible in order to maintain a consistent coordinate system. Neither the projected spatial centroid nor the mean velocity is weighted by the luminosity, because we do not want to introduce an a priori bias toward the brightest group galaxy or assume implicitly that the mass-to-light ratios for all group members are the same. Nevertheless, the luminosity-weighted centroids are within 2σ of the unweighted centroids for all groups except B1422 (where four bright galaxies close to the lens pull the luminosity-weighted centroid 3.5σ away from the unweighted centroid).

4.3.1. *Projected Offset Between the Spatial Centroid and the Lens Galaxy*

If a group around a lens has a common dark matter halo, the effects of that halo on the lens potential are sensitive to any projected spatial offset between the halo centroid and the lens galaxy. In particular, the offset determines the relative importance of convergence (gravitational focusing) and shear (tidal distortions) from the group halo. (See §4.4 and the Appendix for details.) While we obviously want to determine the offset in each lens/group system, we also seek to understand the distribution of offsets because that affects the distribution of convergence and shear, which in turn affects statistical applications like constraining the dark energy or understanding the quad/double ratio. For MG0751, PG1115, and B1422, the new members we have found allow us to measure the offsets more precisely. For the newly discovered groups around BRI0952, MG1654, and B2114, we are able determine the offsets for the first time.

Figure 4 shows that in some cases there is a clear offset between the lens galaxy and the projected group spatial centroid. In B1422, the offset is substantial; the lens galaxy lies outside the 2σ errors for the group centroid and is not the galaxy closest to the group centroid. In MG0751, PG1115 and MG1654 the lens galaxy is only marginally within the 2σ centroid errorbars, and is also not the galaxy closest to the centroid. We use these spatial offsets in our calculations of the shear and the convergence due to the lens environment in §4.4.

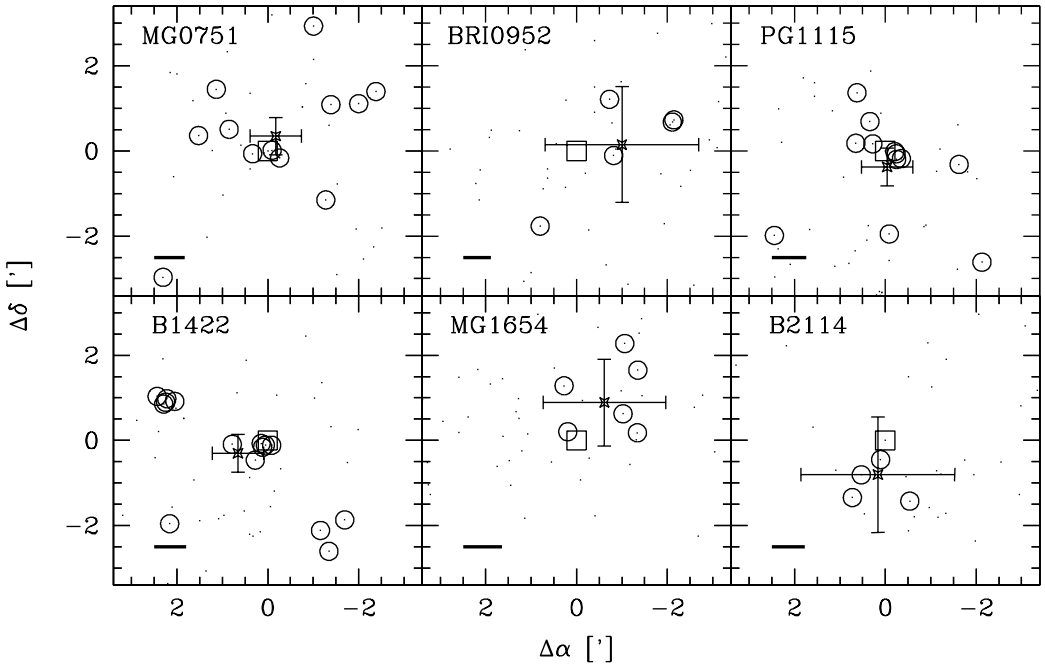

FIG. 4.— Spatial distribution of the group member galaxies on the sky. North is up and east is to the left. The fields are centered on the lens. Each panel has an angular size of $6.8' \times 6.8'$, which is roughly equivalent to the typical size of nearby poor groups. The open circles mark the group galaxies, an open square denotes the lens galaxy, and a four-pointed star indicates the group centroid and its 2σ errorbars (see §4.3). All galaxies with measured velocities are marked with small solid points. The scale bar in the lower left corner of each panel corresponds to 200 kpc at the lens redshift.

4.3.2. *Brightest Group Galaxy vs. Group Potential*

Key issues that bear on the evolution of groups and their galaxies are whether the brightest group galaxy (hereafter BGG) is kinematically and spatially distinct from (1) the other group members or (2) from the center of the group potential. In nearby X-ray luminous groups ($\sigma_r \gtrsim 300$ km s^{-1}), there is a bright, giant elliptical galaxy that occupies the center of the potential (as defined by the spatial and kinematic centroids) and that lies on an orbit distinct from the other group members (ZM98). Our survey now allows us to ask the same questions for intermediate-redshift groups, and to consider what the answers imply about group evolution.

In each of our six groups the BGG appears to have an early-type morphology. The identifications are as follows:

- MG0751: The BGG is the G1 galaxy, which lies $6''$ from the lens galaxy and is 2.2 mag brighter in I. Lehár et al. (1997) fit elliptical profiles to G1 and find an acceptable fit. Furthermore, Tonry & Kochanek (1999) find that G1 is much brighter that the lens galaxy and has a pure absorption line spectrum.
- BRI0952: We identify the BGG by visual inspection of our photometry as an elliptical $2.3'$ away from the lens galaxy and 1.5 mag brighter in I.
- PG1115: The BGG is the giant early-type galaxy labeled G1, located $12''$ away from the lens galaxy and 0.7 mag brighter in I. Impey et al. (1998) comment on its early type morphology.
- B1422: Kundić et al. (1997b) claim the BGG is the galaxy G3 located $8''$ from the lens galaxy and 1.5 mag brighter in V. It is the brightest group galaxy in our sample, has a central location, and exhibits an early type spectrum.
- MG1654 and B2114: In both cases, the lens galaxies are the brightest galaxies in the groups and are also ellipticals as classified by Kochanek (1995) and Augusto et al. (2001), respectively.

The top panel of Figure 5 shows the projected spatial x and kinematic y offsets from the group centroid for the BGGs (filled squares) and for all other member galaxies (filled circles) in our sample groups. The y errorbars (ϵ_y) represent the 1σ uncertainties based on adding the galaxy velocity errors and the group mean velocity errors in quadrature. The x errorbars (ϵ_x) represent the 1σ uncertainties based on the adding the centroid errors and the individual galaxy position errors in quadrature (the centroid errors dominate). To estimate the statistical errors of the centroid for a group of $N_{\rm grp}$ members, we carry out a statistical bootstrap analysis where we draw 500 random samples of $N_{\rm grp}$ galaxies without replacement from the B1422 group (the one with the most members), and adopt the variance of the centroid position as its error. For B1422, we use the smallest of the

errors calculated for the other groups.

We define the quantity $R^2 = (x/\delta_x)^2 + (y/\delta_y)^2$ as a measure of the phase-space distance of a galaxy from the group centroid. Here δ_x and δ_y are the rms deviations in x and y for all galaxies plotted in the top panel of Figure 5. A galaxy will have a large value of R if it has a large peculiar velocity and/or a position that is far from the projected spatial centroid. Conversely, galaxies at rest in the center of the group potential will have small R values. The bottom panel of Figure 5 shows the distributions of R values for the BGGs (shaded histogram) and for all other group members (unshaded histogram). We can now use these distributions to answer two questions about the BGGs.

Are the BGGs distributed differently than the other group galaxies? We compute the R distributions for BGGs and for all other group galaxies (see the bottom panel of Figure 5), and then compare them using three statistical tests: the KS-test (to compare the overall distribution), the t-test (to compare the means), and the F-test (to compare the variances). All three fail to distinguish between the two distributions. In other words, there are no significant differences between the orbits of BGGs and the orbits of other group members, at least for these small samples. This result differs from observations of nearby groups (see ZM98). It is not clear from our present sample whether our result indicates real evolution in the group galaxy population between $z \sim 0.3$ and $z = 0$, or is due simply to small number statistics. It will be interesting to return to this question with the larger sample of lensing-selected groups that we are obtaining.

Are the BGGs consistent with the group centroids? We compare the distribution of R values for the BGGs with a model distribution expected for a galaxy lying at the bottom of the group potential. To incorporate measurement errors, we treat the model distribution as a Gaussian in x and y with rms deviations of ϵ_x/δ_x and ϵ_y/δ_y, respectively, and make 1000 random draws using the appropriate values of ϵ_x and ϵ_y for each group. The bottom panel of Figure 5 shows the observed and model distributions. A KS-test gives 6.6×10^{-3} as the probability that the two samples are drawn from the same distribution. The probability that the means of the two distributions are the same is 7×10^{-9}, while the probability that the variances are the same is 10^{-5}. We conclude that the BGGs do not occupy the center of the group potential.

This offset of the BGG from the kinematic and spatial centroid of the group is not seen in nearby X-ray luminous groups. While our result could suggest group evolution from $z \sim 0.3$ to now, another possibility is that we are not comparing apples to apples. For example, there are groups in our sample with velocity dispersions lower than what is typical for dynamically-evolved X-ray luminous groups nearby. Among nearby groups, lower-σ_r systems tend to be dynamically younger and are more likely to have an offset BGG (e.g., the Local Group). This may be true among our $z \sim 0.3$ groups as well.

Support for this latter interpretation comes from a closer look at the BGGs in the three high-σ_r groups in our sample: B1422, PG1115, and MG0751. The BGGs of MG0751 and PG1115 are the galaxies closest to the projected spatial/kinematic centroid in their respective groups, and, within the errors, are consistent with being at the centroid. In contrast, the BGG in B1422 lies at a large projected distance from the projected spatial centroid ($\sim$0.22 Mpc) and has a substantial peculiar velocity (1270 km s^{-1}). The BGG spatial and kinematic offset, together with the clumpiness of B1422 (see §4.1), suggest that this system is not yet relaxed. Therefore, in two out of three cases, the high-σ_r groups in our sample are comparable to those nearby groups with high velocity dispersions and centrally located BGGs.

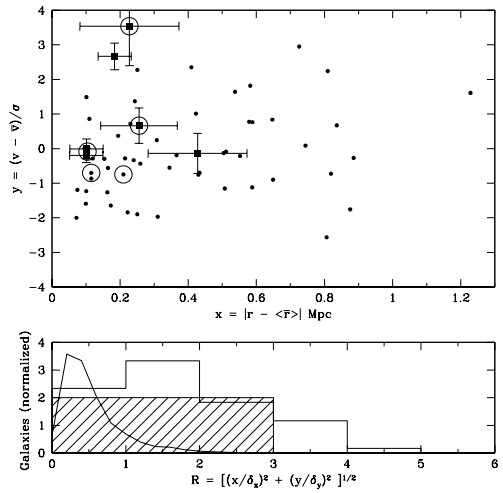

FIG. 5.— *(Top)* Projected spatial and kinematic offsets of the brightest group galaxy (BGG; filled squares) and all other group members (filled circles) from the group centroid for five of our groups. The lens galaxies are marked with open circles. (The lens galaxy in BRI0952 is omitted because it does not have a measured redshift.) The velocity offset is normalized by the velocity dispersion of the group to compensate for the differences among the group potentials. The y errorbars represent the 68% confidence level based on adding the errors for the lens galaxy velocity and the mean group velocity in quadrature. The x error bars are the 68% confidence level based on a statistical bootstrap test (see text). *(Bottom)* Distribution of the phase-space offset R for the BGGs (shaded histogram) and all other group galaxies (open histogram, normalized by the number of the brightest group galaxies). Statistical tests fail to distinguish between these two distributions. The heavy line (scaled down by a factor of 400 to fit the y-axis) shows the model R distribution for a galaxy assumed to lie at the bottom of the group potential (see text). A KS-test gives 7×10^{-3} as the probability that the BGG and model distributions are drawn from the same parent distribution, and a t-test gives 7×10^{-9} as the probability that the means of the BGG and model distributions are the same. We conclude that the BGGs generally do not occupy the center of the potential, and, that, within the large uncertainties, their phase space distribution is consistent with that of the other group members.

We also compare the projected spatial centroid with the peak of emission from the diffuse, luminous X-ray halos in PG1115 and B1422 (the two highest-σ_r groups) seen by Grant et al. (2004). In PG1115, the projected spatial centroid and X-ray peak are consistent within 2σ. By contrast, in B1422 the peak of the X-ray emission is substantially offset (more than 3σ) from both the unweighted and luminosity-weighted group centroids.

Our ability to address the questions of evolution raised in this section will improve when we finish obtaining the larger sample of lensing-selected groups. Since lensing is sensitive to groups spanning the redshift range $0.2 \lesssim z \lesssim 1$, it will naturally provide the large red-

shift baseline needed to probe evolution. Working with a self-consistently selected sample of groups will mitigate selection effects.

4.4. *Group Contributions to Lens Potentials*

The understanding of environment-related biases and uncertainties in lensing constraints on the masses and shapes of galaxy dark matter halos, H_0, and substructure requires detailed lens modeling (see KZ04). That is beyond the scope of this paper and will be treated separately. For our purposes here, a simple way to quantify environmental effects is to determine the dimensionless convergence κ and shear γ that the group contributes to the lens potential. The convergence represents gravitational focusing created by additional mass at the position of the lens galaxy, while the shear represents tidal distortions created by having an inhomogeneous distribution of matter near the lens galaxy. Convergence can never be constrained using lens models alone because of the mass sheet degeneracy (Gorenstein et al. 1988; Saha 2000). As a result, it is often omitted, which can lead to significant biases in the model results (KZ04). Shear cannot be constrained in models of two-image lenses, which leads to enormous model uncertainties. While shear can be constrained in models of four-image lenses, one of the puzzling results is that shear is required in nearly all four-image lenses, and the required shear strengths cannot easily be explained by traditional models of large-scale structure (Keeton et al. 1997; Dalal & Watson 2004).

Models of four-image lenses lead to the rule of thumb that a shear of $\gamma \sim 0.1$ is common for groups, and $\gamma \sim 0.3$ for clusters. Generally, we expect $\kappa \geq \gamma$ because of the way convergence and shear add when there is more than one perturber (see the Appendix). Many lensing conclusions scale as $(1-\kappa)$ to some power (see KZ04 and the Appendix), which can help us estimate the biases. For example, if a lens has convergence $\kappa \sim 0.1$, then lens models that omit the convergence will overestimate H_0 by $\sim$10%. Hence, we consider convergences and shears larger than $\sim$0.1 to be quite important, and values down to $\sim$0.05 worth consideration.

In this section, we quantify the effect of the group environments in our sample by determining the convergence and shear due to the group surrounding each lens galaxy. Because it is not clear how the mass is divided between the individual group members and a common group dark matter halo, we consider two extreme cases that bound the range of possibilities. In the "group halo limit," we assume that all of the mass is associated with a common group halo, and we estimate the amount of mass from the velocity dispersion. In the "group galaxies limit," we assume that all of the mass is bound to the individual member galaxies, and we calibrate the individual shears and convergences with recent weak lensing observations (Sheldon et al. 2005). Comparing results from the two limits can indicate how much our conclusions depend on how the mass is distributed within the group.

4.4.1. *Group Halo Limit*

The group halo limit is appropriate for considering relaxed, dynamically evolved groups in which the individual dark matter halos of member galaxies may have been stripped by interactions, so that the dominant component is a common dark matter halo. In this case, the luminous galaxies just trace the underlying mass distribution, and the velocity dispersion of the galaxies is a measure of the mass of the group as a whole. If we model the group halo as a singular isothermal sphere (SIS), then we can take the velocity dispersion σ_r of a group and its centroid position (b, ϕ) in polar coordinates centered on the lens galaxy, and compute the convergence $\kappa_{\rm grp}$ and shear $\gamma_{\rm grp}$ using eq. (A20) in the Appendix. (Note that $\kappa_{\rm grp} = \gamma_{\rm grp}$ in the SIS approximation.) We then use the uncertainties in the velocity dispersion and centroid position to determine the uncertainties in the convergence and shear. These derived uncertainties are highly non-Gaussian, so we compute them using Monte Carlo simulations.

The results are presented in Table 5.[4] *In three of the six groups (MG0751, PG1115, and B1422), the convergence and shear are significant.* In these systems the group environment needs to be accounted for in lens models, and our measurements of the group properties make that feasible. In the other three groups (BRI0952, MG1654, and B2114), it appears from our current data that the convergence and shear are small.

The case of B1422 illustrates how our identifications of additional group members affect estimates of the convergence and shear. Based on six members, Kundić et al. (1997b) estimated that the group velocity dispersion is $\sigma_r = 550$ km s^{-1}, and that the centroid lies a projected distance of $b \sim 14''$ from the lens galaxy. That led them to estimate a large "observed" shear of $\gamma_{\rm obs} = 0.23$, a value consistent with the shear $\gamma_{\rm mod} \sim 0.2$ required by lens models (Hogg & Blandford 1994; Keeton et al. 1997; Dobler & Keeton 2005). Now with 16 members, we find a smaller velocity dispersion $\sigma_r = 470$ km s^{-1} and a larger offset $b = 43''$, which reduce the nominal observed shear to a more moderate value of $\gamma_{\rm obs} = 0.058$. Accounting for the measurement uncertainties (which has not been done before), we find allowed ranges of $0.034 \leq \gamma_{\rm obs} \leq 0.095$ at 1σ, and $0.020 \leq \gamma_{\rm obs} \leq 0.170$ at 2σ. It is clear that omitting the group members can bias the estimates of how the environment affects the lens potential. However, even with an extensive catalog (16 members), uncertainties are important when comparing observations of the group with inferences from lens models. The large difference between the nominal observed shear $\gamma_{\rm obs} = 0.058$ and the shear required by models $\gamma_{\rm mod} \sim 0.2$ might not be significant at more than 2σ. To test consistency between the observations and models, it is best to make new models with the environment constrained by our observations (including the uncertainties, and possible clumpiness within the group; see §4.1).

4.4.2. *Group Galaxies Limit*

In the group galaxies limit, we suppose that all the mass in the group is bound to the individual member galaxies. This is probably a better approximation for dynamically younger groups, which may still be in the process of collapse and whose galaxies still retain their halos.

To calibrate the shear and convergence from each galaxy, we turn to observations that are perfectly suited

[4] As noted in the table caption, we assume $z_s = 2$ for the unknown source redshift in B2114, but the particular value has little effect on our results.

TABLE 5
Convergence and Shear in the Group Halo Limit

Lens	b [$''$]	σ_r [km s^{-1}]	$\kappa_{\rm grp} = \gamma_{\rm grp}$	θ_γ [deg]	Number of Images
PG1115	23	440	$\mathbf{0.089}\ ^{+0.065}_{-0.046}$	6 ± 37	4
B1422	43	470	$\mathbf{0.058}\ ^{+0.037}_{-0.024}$	-65 ± 20	4
MG0751	23	320	$\mathbf{0.049}\ ^{+0.071}_{-0.033}$	-27 ± 36	4+R
MG1654	65	200	$0.007\ ^{+0.011}_{-0.005}$	-35 ± 30	R
BRI0952	61	170	$0.005\ ^{+0.013}_{-0.004}$	-81 ± 42	2
B2114[a]	49	110	$0.003\ ^{+0.014}_{-0.002}$	-12 ± 52	2

Note. — The groups are sorted by decreasing values of the convergence and shear. The magnitudes of the convergence and shear are equal ($\kappa_{\rm grp} = \gamma_{\rm grp}$) in the SIS approximation. Values larger than 0.05 are marked in boldface. The angle θ_γ defines the direction of the shear (measured North through East). The convergence and shear errorbars are 1σ uncertainties derived from the uncertaintines in the group centroid position and velocity dispersion (from Table 4). Column 6 lists the image configuration for each lens: 2-image, 4-image, or ring (R).

[a]We assume a source redshift $z_s = 2$ for B2114, but the particular value has little effect on our results. In particular, assuming $z_s = 3$ leads to the same numerical values for the $\kappa_{\rm grp}$, $\gamma_{\rm grp}$, and θ_γ.

to our needs: weak lensing. The advent of large surveys, such as the Sloan Digital Sky Survey, has made it possible to measure shear as a function of distance from an average galaxy, on scales from 20 h^{-1} kpc to 7 h^{-1} Mpc (e.g., Sheldon et al. 2005).[5] The projected offsets of galaxies in our sample range over $\sim$ 20–700 h^{-1} kpc, so we are working in precisely the regime studied by Sheldon et al. (2005). One possible concern with this calibration is that the Sheldon analysis provides limited information about how shear and convergence scale with luminosity (or mass). Sheldon et al. (2005) measured the shear profile in three luminosity bins, but most of our galaxies fall into just one of the bins ($-22 < M_i - 5\log h < -17$). Thus, we expect that our present analysis characterizes the average properties of the group galaxies well, but it will be worthwhile to redo the analysis when future weak lensing data provide finer luminosity resolution.

The quantity that is measured in weak lensing studies is shear, but the observed shear profile is consistent with a power law which means that there is a simple relation between the shear and convergence. The Appendix gives this relation, and also provides more details about how we use the weak lensing data to calibrate our analysis.

Once we have computed the convergence and shear from each galaxy, we combine them in the manner of eqs. (A12)–(A16) in the Appendix. The net convergence and shear for each group are presented in Table 6. We also list statistical uncertainties derived (using Monte Carlo simulations) from the errorbars on the weak lensing parameters quoted by Sheldon et al. (2005). These are generally small and are probably less important than systematic effects due to incompleteness (see below). As in the group halo limit, in the galaxies limit we find that MG0751, PG1115, and B1422 all have significant group contributions to the lens potential. The group contributions are fairly small in MG1654, BRI0952, and B2114. Comparing Tables 5 and 6 leads to a crucial point: our conclusions about which groups significantly affect the lens potentials do not depend on assumptions about how the mass is distributed within the groups. While the detailed lensing implications do depend on the mass distribution — which is actually useful (see §4.4.3) — it is reassuring to see that our qualitative conclusions about which groups are important for lensing are robust.

In carrying out this analysis we do not distinguish between different morphological galaxy types. Given their higher mass-to-light ratios, elliptical (red) galaxies would produce more shear and convergence than spiral (blue) galaxies of the same luminosity. To test the effects of morphology on our results we consider the extreme assumption that all group galaxies are red and use the Sheldon et al. (2005) shear profiles for red galaxies. In almost all cases the total convergence and shear due to the group increase by $\sim$70%. Thus, if most group members are red galaxies then our current analysis may actually underestimate the convergence and shear by as much as 70%.

As a simple sanity check, in Table 6 we also compute the net convergence and shear assuming that each galaxy can be treated as a singular isothermal sphere (SIS) with velocity dispersion $\sigma = 100$ km s^{-1}. We expect that many of the galaxies have larger velocity dispersions, and given that convergence and shear scale as σ^2, this simple case should provide a conservative lower bound on the net convergence from the group. (The shear is more complicated, as discussed below.) Comparing the results assuming $\sigma = 100$ km s^{-1} with those based on the weak lensing calibration confirms this expectation, and generally suggests that the weak lensing calibration is reasonable. We should note that the convergence from the simple SIS model may not be a strict lower bound if halos are significantly truncated, but in practice most of the convergence (and shear) arise from galaxies close enough

[5] Sheldon et al. (2005) quote comoving distances, but we have converted to angular diameter distances as those are more natural for our analysis.

TABLE 6
Net Convergence and Shear in the Group Galaxies Limit

Lens	[Sheldon] $\kappa_{\rm tot}$	[Sheldon] $\gamma_{\rm tot}$	[Sheldon] θ_γ [deg]	[$\sigma = 100$ km s^{-1}] $\kappa_{\rm tot}$	[$\sigma = 100$ km s^{-1}] $\gamma_{\rm tot}$	[$\sigma = 100$ km s^{-1}] θ_γ [deg]
PG1115	$\mathbf{0.066}^{+0.012}_{-0.006}$	$0.028^{+0.009}_{-0.003}$	64.2 ± 3.2	0.040	0.031	66
B1422	$\mathbf{0.092}^{+0.019}_{-0.009}$	$0.010^{+0.012}_{-0.004}$	$-35.6^{+25.4}_{-13.5}$	**0.064**	0.019	-34
MG0751	$\mathbf{0.115}^{+0.040}_{-0.026}$	$\mathbf{0.091}^{+0.057}_{-0.034}$	-82.9 ± 1.8	0.040	0.029	-88
MG1654	$0.027^{+0.006}_{-0.004}$	$0.006^{+0.005}_{-0.003}$	21.4 ± 13.2	0.013	0.004	43
BRI0952	$0.013^{+0.002}_{-0.002}$	$0.007^{+0.001}_{-0.001}$	-64.6 ± 8.3	0.006	0.003	-67
B2114[a]	$0.016^{+0.004}_{-0.002}$	$0.012^{+0.003}_{-0.002}$	-15.9 ± 3.3	0.008	0.007	-16

Note. — The groups are sorted as in Table 5. Values larger than 0.05 are again marked in boldface. Columns 2–4 list the net convergence and shear when we calibrate the individual galaxies using the weak lensing observations by Sheldon et al. (2005). The errorbars represent 1σ statistical uncertainties derived from the weak lensing errorbars quoted by Sheldon et al.; even more important may be systematic effects due to spectroscopic incompleteness (see text). For a simple comparison, Columns 5–7 list the results when we treat each galaxy as an isothermal sphere with velocity dispersion $\sigma = 100$ km s^{-1}.

[a]Again, we assume a source redshift $z_s = 2$ for B2114, but the particular value has little effect on our results.

to the lens that truncation would have little effect. For example, if all halos had cut-off radii at 300 kpc, the SIS model convergence would drop from $\kappa = 0.040$ to 0.036 in PG1115, and from 0.064 to 0.057 in B1422. Even with an extreme cut-off at 100 kpc, the convergences would still be 0.027 for PG1115 and 0.051 for B1422. (In all cases, the shears are basically unchanged.) We expect that the conservative assumption of a small velocity dispersion more than compensates for the omission of a cut-off radius, so that the SIS model results are indeed lower bounds.

It is again interesting to consider how our efforts to increase the group membership have affected conclusions about the convergence and shear. The most instructive case is PG1115. With our catalog of 13 members, we find a net convergence $\kappa = 0.066^{+0.012}_{-0.006}$ and a net shear $\gamma = 0.028^{+0.009}_{-0.003}$ at position angle $\theta_\gamma = 64 \pm 3$. If Kundić et al. (1997a) had done the same analysis with their catalog of four members, they would have found $\kappa = 0.027^{+0.008}_{-0.005}$, $\gamma = 0.014^{+0.006}_{-0.003}$, and $\theta_\gamma = 69 \pm 5$. (Tonry 1998 would have obtained similar results.) In other words, the previous catalogs missed at least half of the sources of shear and convergence. The problem was that they focused on the region within $\sim 30''$ of the lens, but (in the galaxies approach) the galaxies have extended dark matter halos, requiring the inclusion of group members out to the full virial radius of the group in order to fully characterize environmental effects in lens models.

With this thought in mind, we must consider how spectroscopic incompleteness may affect the results in Table 6. We cannot account for galaxies that we missed, but we can ask how our results would have differed had we omitted a few of the galaxies that we did actually include. The effects of incompleteness on the net convergence are simple: since convergences from different galaxies combine in a simple scalar sum (see eq. A12 in the Appendix), omitting galaxies causes us to underestimate the net convergence. Turning this around, we can say that our estimates of $\kappa_{\rm tot}$ are strict *lower bounds* on the convergence from the group. To be more quantitative, in analyzing subsamples of our group catalogs we find that the net convergence scales roughly with the number of group members; so if the true number of members is, say, 50% larger than what we have observed then we expect the true convergence to be $\sim$50% larger than our estimate. For understanding biases in lens models, it is very valuable to have a lower bound on the total convergence, because that can be turned into lower bounds on the biases.

The shear is more complicated, because multiple contributions sum as tensors rather than scalars (see eqs. A13 and A14); adding more contributions can either increase or decrease the net shear, and modify the position angle. The effects depend on the spatial distribution of member galaxies. In PG1115 the most important galaxies lie roughly in a line on the sky, which means that the direction of the net shear is robust against incompleteness, while the amplitude of the shear scales roughly with the number of group members. In contrast, in B1422 the galaxies are distributed more broadly, so incompleteness may change the shear direction by tens of degrees and the shear amplitude by tens of percent. (Of course, the shear from the galaxies in B1422 is small, so even large fractional uncertainties are not so important.) Finally, in MG0751 the environmental effects are dominated by the galaxy G1 that is massive and close to the lens.

The bottom line is that incompleteness does not significantly affect our qualitative conclusions. Since our estimate of the net convergence is a lower bound, we know that our conclusion that groups are important on MG0751, PG1115, and B1422 is robust. While it is possible that our conclusion that the groups are not so important in MG1654, BRI0952, and B2114 could change if we measure more galaxies and find that κ rises, the observed correspondence between th group velocity dispersion and richness (see §4.2) suggests that adding more members would not affect κ significantly. Incompleteness

issues will need to be considered when making detailed quantitative comparisons between our environment observations and lens models.

4.4.3. *Discussion*

It is important to understand the similarities and differences between the results from the "group halo" and "galaxies" limits. We have already noted that both limits lead to the same conclusions about which groups are important for lensing. All three high-σ_r groups (MG0751, PG1115, and B1422) produce a significant convergence in both approaches, so these groups cannot be ignored in lens models. At the same time, two of the low-σ_r groups (BRI0952 and B2114) produce a small shear and convergence in both approaches, suggesting that these groups are not so important for lensing. While this latter conclusion may not seem exciting, it is actually quite valuable. Two-image lenses (including both BRI0952 and B2114) suffer from a strong degeneracy between ellipticity and shear, if both quantities are unknown. That degeneracy can now be broken by ruling out models with large shear. The situation is less clear for MG1654, because the group halo analysis implies negligible shear, while the galaxies analysis yields a small but non-negligible shear $\gamma = 0.03$ (and that could be an underestimate).

When we turn to a more quantitative comparison of the two approaches, we notice some significant differences. The differences suggest that it may be possible to distinguish between the group halo and galaxies limits, and thus to learn about the distribution of dark matter within the groups. For example, in B1422 the group halo analysis leads to a moderate convergence and shear, while the galaxies analysis leads to a larger convergence but a negligible shear. Lens models require a large shear $\gamma \sim 0.2$ that is marginally consistent with the group halo approach (given our uncertainties) but grossly inconsistent with the galaxies approach. In PG1115, as in B1422, lens models require large external shear $\gamma \sim 0.1$ (Impey et al. 1998). The group halo limit result ($\gamma = 0.089^{+0.065}_{-0.046}$) is within 1σ of the model requirement while the galaxies limit gives a factor of three lower shear, inconsistent with predictions. The results in both B1422 and PG1115 — the two highest velocity dispersion groups — suggest that the mass is distributed in a common halo rather than being attached to the individual group members (as might be expected if high velocity dispersion groups are more dynamically evolved). This hypothesis needs to be examined more carefully with detailed lens models; rather than just comparing the shear required by lens models with that inferred from our observations, it is important to build models that explicitly incorporate the environment (which may even consist of multiple subgroup halos; see §4.1) in both the group halo and galaxies limits and see whether either case can fit the lens data. Systems like B1422 and PG1115 may provide an exciting opportunity to determine the distribution of dark matter in a distant group.

We also note that KZ04 used PG1115 as a fiducial example with which to asses environment-related biases in lens models. Dalal & Watson (2004) suggested that PG1115 is a very atypical lens environment, and that KZ04 therefore overestimated environmental effects. To the contrary, we find that PG1115 is nothing if not typical: the group's kinematic properties and shear and convergence are consistent with at least half of the groups in our sample.

Another interesting system is MG0751. Here, the galaxies analysis is dominated by the G1 galaxy, lying just $6''$ from the lens. Even so, Lehár et al. (1997) showed that lens models including only the lens galaxy, G1, and up to three other nearby galaxies cannot fit the lens data. It will be interesting to use new lens models to test the hypothesis that both G1 and the common group halo contain significant mass, and to see whether we can constrain their relative masses. We must issue two warnings, however. First, the projected offset of G1 from the lens galaxy is just 20 h^{-1} kpc, which lies at the inner limit of the range studied by Sheldon et al. (2005); thus, the reliability of the weak lensing calibration is not clear. Second, we show in §4.5.2 that MG0751 also has a significant shear from a group along the line of sight, which must be included in lens models along with the group at the lens redshift.

In summary, our results above show that: (1) Group environments, whether the mass lies with individual member halos (galaxies limit) or in a common group halo (group halo limit), can contribute significantly ($\kappa, \gamma \geq 0.05$) to the lens potential. (2) If the members have halos (galaxies limit), they can have a big effect, perhaps even greater than that of a common group halo. (3) In the galaxies limit, correcting for incompleteness is only going to boost the convergence (but will move the shears in either direction). (4) In the highest velocity dispersion groups, the shears produced in the group halo limit are more consistent with the observationally required values, suggesting that we might be able to discriminate between the models of the mass distribution.

Finally, it is remarkable that the three lenses with significant environmental effects include both quad lenses (PG1115 and B1422) and the one quad/ring (MG0751), whereas the double/ring (MG1654) and the two double lenses (BRI0952 and B2114) all have small convergence and shear. While this result is limited by small number statistics, it may suggest a correlation between image configuration and environment. Conventional wisdom (e.g., Rusin et al. 2001) holds that shear does not significantly affect the relative numbers of quads and doubles. However, KZ04 argue that treating environment properly (including terms beyond a simple shear) does change the quad/double ratio. Our new results provide empirical evidence that there is a connection.

4.5. *Lensing Effects of Line-of-Sight Structures*

Since lensing is a projected phenomenon, we must consider whether structures projected along the line of sight significantly affect strong lens systems. Different theoretical approaches to studying the effects of interlopers on strong lensing in a ΛCDM universe have yielded contradictory results (e.g., Bar-Kana 1996; Keeton et al. 1997; Premadi & Martel 2004; Wambsganss, Bode & Ostriker 2004), so an empirical approach is clearly necessary. To date, there are only three lenses with confirmed line-of-sight groups (B0712+472, B1608+656 and MG 1131+0456; Fassnacht & Lubin 2002; Tonry & Kochanek 2000; [Fassnacht et al. 2005) and several other candidates (Faure et al. 2004; Morgan et al. 2005). Here we present the first systematic survey for structures along the

line-of-sight to strong lens systems. The large redshift baseline and wide field of view of our spectroscopic survey make it ideally suited to address this issue.

4.5.1. *The Zone of Influence*

Our first task is to estimate the "zone of influence" for a perturber along the line of sight to each lens in our sample. Although it has not been done before, the calculation is straightforward using the formalism presented in the Appendix. Briefly, if we assume that a perturber can be modeled as an isothermal sphere with some given velocity dispersion, then we can use eqs. (A6), (A7), and (A20) to compute the effective convergence and shear ($\kappa_{\rm eff}$ and $\gamma_{\rm eff}$) as a function of the impact parameter b of the perturber relative to the lens, and the redshifts of the lens galaxy and perturber. (In the SIS approximation, $\kappa_{\rm eff} = \gamma_{\rm eff}$ for a single perturber.)

Figure 6 shows contours of $\kappa_{\rm eff} = \gamma_{\rm eff}$ in the plane of b and $\Delta z = z_{\rm pert} - z_{\rm lens}$, for perturbers with velocity dispersions of 100, 300, or 500 km s^{-1}. (Because we do not see rich clusters along the lines of sight to these lenses, this range of σ_r should span the observed range of structures.) The grayscale is explained in the figure caption. We consider the zone of influence to be the region in which $\kappa_{\rm eff}, \gamma_{\rm eff} \geq 0.05$, i.e., the unshaded (white) region in the figure. The shape of this region is not sensitive to the fact that an SIS halo has an infinite extent; a cut-off halo radius of 300 kpc does not change the zone of influence. Also interesting are regions in which $\kappa_{\rm eff}$ and $\gamma_{\rm eff}$ go negative (shaded black), which represents a breakdown of our formalism. This happens only when the intrinsic convergence of the perturber is $\kappa > 0.5$, which means that the offset between the lens and perturber is small enough that the lens actually lies within the Einstein radius of the perturber (see the Appendix). In this case, the "perturber" is no longer just a perturbation because its caustics interact with those of the main lens galaxy, and we would observe a strong lensing effect from the second mass as well. This breakdown does not affect our conclusions because we do not actually see any structures lying within this region; besides, any objects that lie so close to the line of sight to the lens would presumably be known from previous observations.

As the velocity dispersion of the perturber increases, the zone of its influence grows dramatically $\propto \sigma_r^2$. Consequently, a more massive perturber can produce a large shear and convergence even when offset from the lens; a perturber with $\sigma_r \sim 500$ km s^{-1} (i.e., a rich group) can be offset by as much as $1'$ and still produce $\gamma \sim 0.05$. Another striking feature of Figure 6 is the very wide redshift baseline in front of and behind the lens over which a perturber can cause significant effects. This result shows that it is crucial to catalog not just mass structures in the immediate vicinity of the lens galaxy, but also elsewhere along the line of sight, in order to model the lenses accurately.

4.5.2. *Prominent Interloping Structures*

To quantify line-of-sight effects for the lenses in our sample, we consider the most prominent structures (those likely to be groups and clusters) identified from our redshift catalog. This approach is analogous to the group halo limit for groups around lens galaxies (§4.4.1),

For figure see file f6_sm.jpg

FIG. 6.— Contours of $\kappa_{\rm eff} = \gamma_{\rm eff}$ produced by a perturber with a velocity dispersion of 100, 300 and 500 km s^{-1}, located at a redshift $0 < z_{\rm pert} < 1$ and having an impact parameter b with respect to the lens, computed for seven of the lenses in our sample. (We exclude PMN2004 because its lens redshift is unknown.) The horizontal axis represents the redshift difference between the perturber and lens galaxy. The vertical axis represents the projected distance of the perturber from the lens, out to $2'$. Contours are drawn at $\kappa_{\rm eff} = \gamma_{\rm eff} = 0.001, 0.01, 0.05, 0.1$ and 0.5, although not all of them are clearly visible in all panels. The grayscale is as follows: $\kappa_{\rm eff}, \gamma_{\rm eff} \geq 0.05$ (white); $0.05 > \kappa_{\rm eff}, \gamma_{\rm eff} \geq 0.01$ (light gray); $0.01 > \kappa_{\rm eff}, \gamma_{\rm eff} \geq 0.001$ (medium gray) and $\kappa_{\rm eff}, \gamma_{\rm eff} < 0.001$ (dark gray). Important regions are $0.5 > \kappa_{\rm eff}, \gamma_{\rm eff} > 0.05$, i.e., the areas in white. At small impact parameter, the perturbation approximation breaks down as we enter a regime in which the perturber itself causes strong lensing (see text); in our calculations, this leads to negative values of $\kappa_{\rm eff}$ and $\gamma_{\rm eff}$ (shaded in black). Notice the strong dependence on σ: the zone of influence scales as σ^2. Massive perturbers can have large effects even when they lie far from the lens. Another striking feature is the very wide redshift baseline in front and behind the lens over which the perturber can cause a significant effect.

because it accounts for the dark matter in massive bound structures. To identify potentially important line-of-sight structures, we show the redshift histograms again in Figure 7, now shading only those galaxies that lie within $1'$ of the lens. We have over-plotted the curve of the normalized shear strength $\kappa_{\rm eff}/\kappa = \gamma_{\rm eff}/\gamma$ (eq. A11) to give an indication of how the convergence and shear vary with redshift. From the discussion in §4.5.1, we expect structures with large velocity dispersions, small projected offsets from the lens, and/or small redshift offsets from the lens galaxy to contribute most to the lens potential. To be conservative, we select only those peaks in Figure 7 that: (1) have at least four members; (2) lie within Δz such that $\kappa_{\rm eff}/\kappa$ and $\gamma_{\rm eff}/\gamma$ are $\gtrsim 0.5$; and (3) have at least one member projected within $1'$ of the lens. For every peak, we set pessimistic 3σ velocity limits and use bi-weight estimators of location and scale to calculate the mean velocity v_i and the line-of-sight velocity dispersion $\sigma_{r,i}$. Based on the membership, we then calculate the projected spatial centroid of the structure, and its offset from the lens galaxy b_i and position angle ϕ_i. Finally, we can use eqs. (A6), (A7), and (A20) to determine the effective shear and convergence.

The results are presented in Table 7. We list the individual effects of all prominent structures. We choose to include the groups at the lens redshifts (repeating results from Table 5), so that we can compare local versus interloping structures. We then sum all structures (using eqs. A12–A16) to obtain the total convergence and shear for each lens (in the group halo limit). We emphasize that our results are conservative in the sense that we have not tallied all the line-of sight objects that might affect the lens models. We do not include galaxies outside prominent peaks and plan to address this question in future work. We have not included all peaks in the velocity histograms (Fig. 7), because most are undersampled or intrinsically poor, and thus have too few members for us to interpret them as likely groups and to compute a

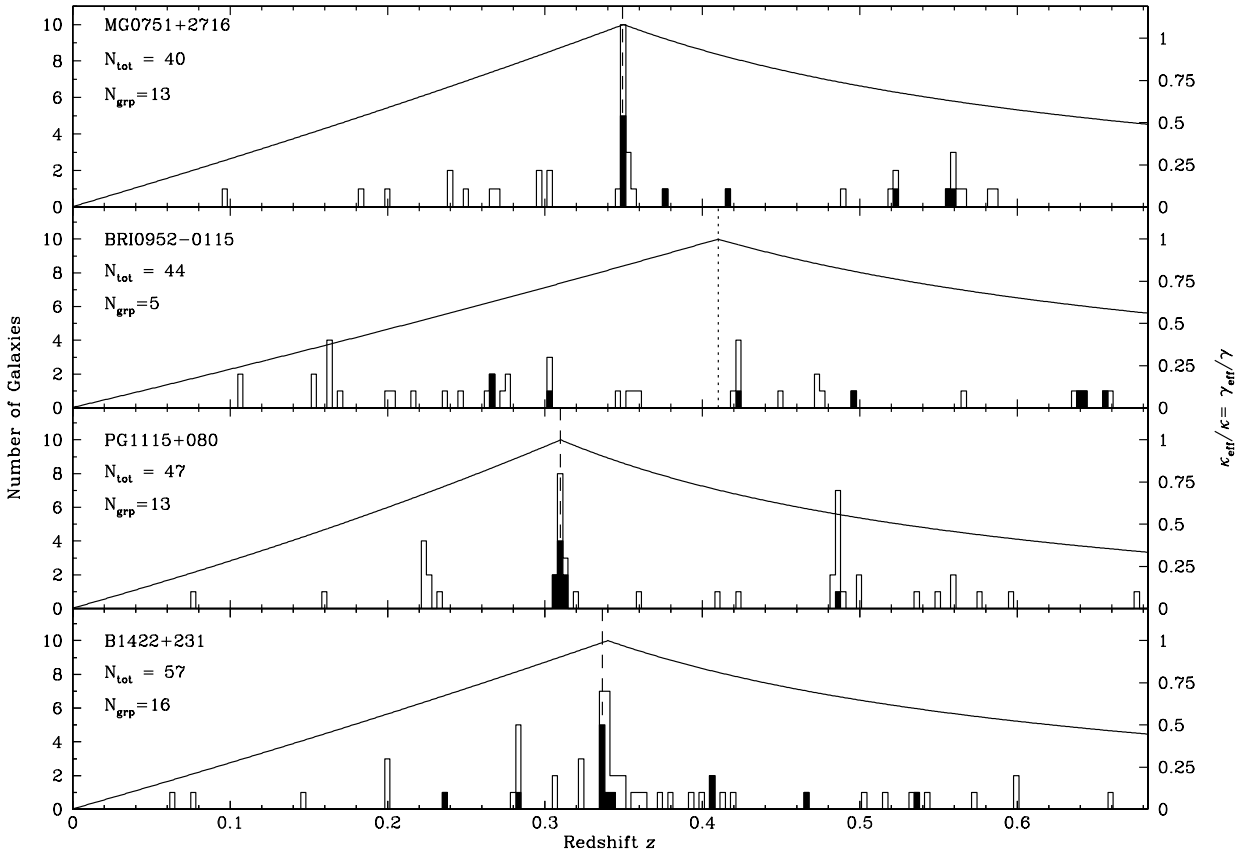

FIG. 7.— Same as the left panels in Figure 3, except that here we have shaded only those galaxies within $1'$ of the lens. We have also overplotted the normalized shear strength and normalized convergence ($\kappa_{\rm eff}/\kappa = \gamma_{\rm eff}/\gamma$; see text) to guide the eye regarding general behavior of convergence and shear as the perturbing structure is moved away from the lens in redshift.

meaningful velocity dispersion. In addition, the velocity dispersions we compute are probably underestimates not only because of the narrow (conservative) choice of initial velocity ranges but also because many of the velocity peaks are poorly sampled. Finally, our spectroscopic target selection prioritizes galaxies thought to lie at the lens redshift (see §3), and to some extent that limits our ability to identify interloping structures.

The discussion of incompleteness in §4.4.2 applies here as well, with one minor change. As before, we note that convergence is a scalar and that the contribution from an overdensity is always positive, and conclude that identifying additional prominent structures would only *increase* the total convergence $\kappa_{\rm tot}$. The change is that an uncertainty in the convergence zeropoint prevents us from declaring that we have obtained a strict lower bound on the total convergence from the line of sight. The zeropoint uncertainty arises from the effects of underdensities such as voids. Strong lensing calculations conventionally assume that there are a few density peaks superposed on top of a smooth background at the mean density of the universe. Voids can then be thought of as regions where the density is negative (relative to the mean), which contribute *negative convergence* to the lens potential (e.g., Seljak 1994). If there is a significant negative convergence, it effectively changes the convergence zeropoint: in summing the effects of overdense structures along the line of sight, we should start not from zero but from the appropriate negative convergence.

We cannot measure the convergence zeropoint directly because that requires knowledge of the local density of matter (dark and luminous) at every point along the line of sight, which is impossible to obtain even with complete redshift surveys. Nevertheless, we can make a useful estimate based on a simple model. We create Monte Carlo simulations of random lines of sight in a universe in which some of the mass is contained in halos while the rest is in a smooth background at a level below the mean density. In these simulations we are able to determine the total convergence $\kappa_{\rm tot}$ from density fluctuations along the line of sight, as well as the contribution $\kappa_{\rm peaks}$ from prominent structures ($\kappa_{\rm peaks}$ is analogous to what we compute above from our data). We can then interpret the difference, $\kappa_{\rm zp} \equiv \kappa_{\rm tot} - \kappa_{\rm peaks}$, as the convergence zeropoint. (Details of the calculation, and further discussion of the results, are given by Keeton et al. 2005b.)

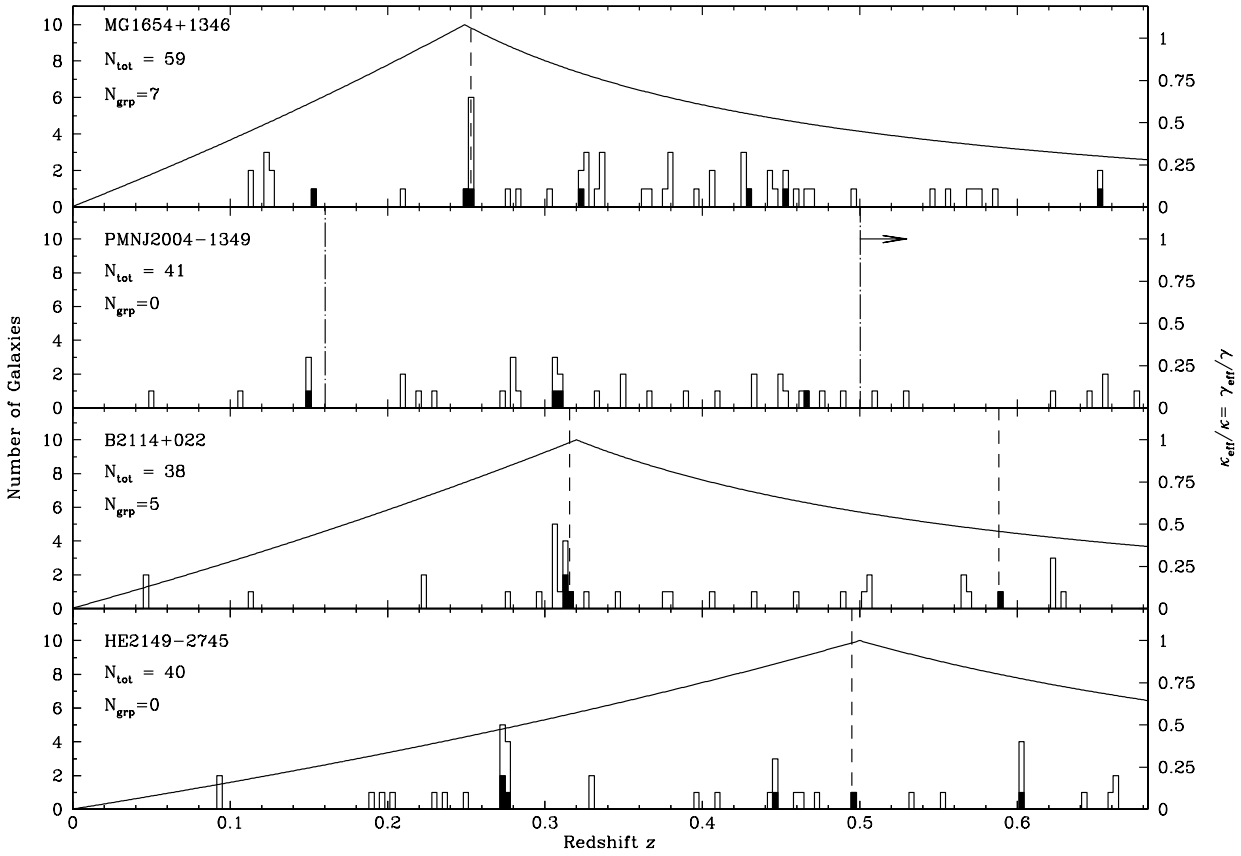

FIG. 7.— continued.

Considering many random lines of sight, we find that $\kappa_{\rm zp}$ has a mean of zero and a dispersion of $\lesssim 0.02$, for typical lens and source redshifts and reasonable halo mass functions. Because the zeropoint uncertainty is small, we believe that our $\kappa_{\rm tot}$ values above are probably lower limits on the total convergence. In other words, it is unlikely that voids contribute enough negative convergence to counter the positive κ from prominent peaks in a given line of sight.

The main result is that four of the eight lenses in our sample have significant interloping structures. MG0751, PG1115, and B1422 each have one structure, and HE2149 has three. At least one of those structures, along the line of sight to MG0751, has a significant contribution to the lens potential. This perturbing group lies at a redshift of $z = 0.56$, which places it between the lens galaxy and the source quasar, and has a velocity dispersion $\sigma_r = 550$ km s^{-1} based on the six members that we have identified. With a centroid that lies at a small projected offset of $28''$ from the lens, the group contributes a convergence and shear $\kappa_{\rm los} = \gamma_{\rm los} = 0.066$. This is clearly an important contribution to the lens potential — in fact, it is slightly stronger than our estimate of the contribution from the group at the lens redshift (in the group halo limit). It represents one more piece in the interesting puzzle of fully understanding lensing in the MG0751 system.

To our knowledge, our lens sample is not biased toward having significant line-of-sight effects. Our survey methods are, if anything, somewhat biased *against* finding line-of-sight structures (as discussed above). Therefore, our discovery of a significant structure in 1/8 lenses suggests that line-of-sight effects are important in at least ∼10% of all lenses. That estimate needs to be confirmed with a larger sample, but it does indicate that lensing effects from the line of sight deserve further attention.

5. CONCLUSIONS

We have presented the first results from our spectroscopic survey of the environments of strong gravitational lenses. We have used multislit spectroscopy to measure the redshifts of 355 galaxies in the fields of eight strong gravitational lenses with lens galaxies at redshifts between 0.25 and 0.50. After adding 16 redshifts from the literature, we have analyzed a total sample of 371 galaxies with redshifts.

The lens galaxy belongs to a poor group in six of the eight systems in our sample. We discover three new groups associated with the lens galaxy of BRI0952 (five

TABLE 7
Convergence and Shear Due to Prominent Line-of-Sight Structures

Lens	ID	$z_{\rm pert}$	b [$''$]	σ_r [km s^{-1}]	$\kappa_{\rm eff} = \gamma_{\rm eff}$	θ_γ [deg]	$\kappa_{\rm tot}$	$\gamma_{\rm tot}$	$\theta_{\gamma,{\rm tot}}$ [deg]
MG0751	1	0.35	23	320	**0.049**	−27			
MG0751	2	0.56	28	550	**0.066**	−56			
MG0751	total						**0.116**	**0.101**	−44
BRI0952	1	0.42	61	170	0.005	−82			
BRI0952	total						0.005	0.005	−82
PG1115	1	0.31	23	440	**0.089**	7			
PG1115	2	0.49	44	300	0.010	−74			
PG1115	total						**0.099**	**0.080**	5
B1422	1	0.34	43	470	**0.058**	−65			
B1422	2	0.28	80	400	0.020	−28			
B1422	total						**0.078**	**0.066**	−57
MG1654	1	0.25	65	200	0.007	−35			
MG1654	total						0.007	0.007	−35
HE2149	2	0.27	51	400	0.017	−62			
HE2149	3	0.45	70	180	0.004	−80			
HE2149	4	0.60	56	150	0.003	88			
HE2149	total						0.024	0.022	−68
B2114	1	0.31	49	110	0.003	−12			
B2114	total						0.003	0.003	−12

Note. — "Prominent" structures are defined as having at least four members, at least one of which is projected within $1'$ of the lens galaxy and displaced by Δz such that $\kappa_{\rm eff}/\kappa = \gamma_{\rm eff}/\gamma > 0.5$. Column 2 labels all the prominent structures along the line of sight to each lens; "0" refers to a group at the lens redshift. (HE2149 is the only lens with more than one interloping structure.) Columns 3–7 refer to individual structures, while Columns 8–10 give the final results after combining all the prominent structures along the line of sight to each lens (including a group at the lens redshift, if there is one). Values larger than 0.05 are marked in boldface.

members), MG1654 (seven members), and B2114 (five members). We more than double the number of members for another three previously known groups around the lenses MG0751 (now 13 members), PG1115 (13 members), and B1422 (16 members). These six groups add to the still small number of all poor groups identified at intermediate redshifts.

We determine the kinematics of the six groups, including their mean velocities, velocity dispersions, and projected spatial centroids. For the newly discovered groups, we quantify these properties for the first time. For the other three groups, the increased membership allows us to make more robust estimates of the kinematic properties of the groups than previously possible. The highest velocity dispersions we measure (320 to 470 km s^{-1} for MG0751, PG1115, and B1422) are consistent with those of nearby dynamically-evolved, X-ray luminous groups (MZ98), while the lower velocity dispersions (110 to 200 km s^{-1}) are more typical of dynamically younger groups at low redshift. In the two cases where a diffuse X-ray component has been measured (PG1115 and B1422; Grant et al. 2004), the X-ray temperatures and our velocity dispersions are consistent with the local σ_r-T_X relation (MZ98).

To understand the evolution of groups and their galaxies, it is important to determine the relation of the brightest group galaxy (BGG) to the group potential. (In four of the six groups, MG0751, BRI0952, PG1115, and B1422, the lens galaxy is not the BGG.) We find that the BGG generally lies off the center of the group potential and occupies an orbit indistinguishable from the other group members. This result is surprising in comparison with nearby, X-ray luminous groups, in which the BGG is always a giant elliptical galaxy occupying the center of the potential, with an orbit distinct from the other group members (ZM98). However, most of the effect we see comes from the three groups with lower velocity dispersions. In two (MG0751 and PG1115) of the three highest velocity dispersion groups, the BGGs lie within the errors of the group centroid, suggesting that at least these systems are comparable to dynamically-evolved poor groups in the local universe.

We use our detailed observations of the groups to assess how environments affect gravitational lens models. A key ingredient is an accurate determination of any offset between the lens galaxy and the group centroid on the sky. In MG0751, PG1115, B1422, and MG1654, the lens galaxy is offset spatially from the group centroid. Obtaining a larger sample (which is underway) to determine the full distribution of lens vs. group offsets will be important for understanding how lens environments affect statistical quantities such as the quad/double ratio and lensing constraints on Ω_Λ (see KZ04).

To quantify environmental contributions to lens potentials in more detail, we estimate the convergence (gravitational focusing) and shear (tidal distortions) from each group. We consider two different models of the group mass distribution that bound the extremes of dynamical states of groups. The members of young groups are likely to still have large dark matter halos and the group mass may be dominated by the dark matter halos of the individual member galaxies. In this approach, we calibrate the shear and convergence from each galaxy based on observations of weak lensing in the Sloan Digital Sky Survey (Sheldon et al. 2005), and then sum the contributions appropriately. As the group evolves, these halos

may be truncated via interactions, so the mass will be redistributed into a common group halo that may be the dominant group mass component. In this approach, we approximate that halo as an isothermal sphere and use the measured group centroid and velocity dispersion to compute the convergence and shear.

At least three of the lenses in our sample (MG0751, PG1115, and B1422) have convergences and shears large enough ($\kappa, \gamma \geq 0.05$) to indicate that the environment plays a significant role in the lens potential. For these systems, our survey substantially improves the observational constraints that will be needed to make detailed lens models that properly include environmental effects. Remarkably, the high shear and convergence values occur in the quad lens systems, while the environments of the double lenses are relatively weak. This result suggests that environment may affect the relative numbers of quad and double lenses, a topic much debated in the literature (see King et al. 1996; Kochanek 1996b; Keeton et al. 1997; Rusin & Tegmark 2001; Cohn & Kochanek 2004; Keeton & Zabludoff 2004). For the other lenses, the conclusion that environment does not significantly affect the lens potential is also valuable: constraining previously unknown environmental terms to be near zero will still improve lens models.

For the first time, we present a systematic assessment of whether structures along the line of sight to lens systems are important for lensing. We show that interloping structures can in principle affect lens models over a wide range of spatial and redshift offsets. Our pencil-beam survey is ideally suited to identifying such structures if they are present. We find that at least four out of eight lenses have prominent line-of-sight structures, i.e., groups whose spatial and redshift offsets place them in the "zone of influence" of the lens. MG0751, PG1115, and B1422 each have one substantial group along the line of sight, while HE2149 has three groups at different redshifts. Of these, the interloping group in MG0751 has a significant effect on the lens potential. Our survey is actually biased against interloping groups (and is not complete), so finding that at least one of eight lenses ($\sim 10\%$) is affected by projected structures is intriguing and worth further study.

We thank the staff of the Magellan Observatory for their tireless efforts on behalf of this project. We appreciate the advice and spectral templates given by Marc Postman, as well as the helpful comments provided by Chris Impey. We thank the anonymous referee for careful and constructive comments. This work was supported by NSF grant #AST-0206084 and NASA LTSA award #NAG5-11108. IM acknowledges the support of the Martin F. McCarthy Scholarship in Astrophysics awarded by the Vatican Observatory.

REFERENCES

Allington-Smith, J. R., Breare, J. M., Ellis, R. S., Parry, I. R., & Shaw, G. D. 1990, Proc. SPIE, 1235, 691
Angonin-Willaime, M.-C., Hammer, F., & Rigaut, F. 1993, Gravitational Lenses in the Universe, 85
Augusto, P., et al. 2001, MNRAS, 326, 1007
Bar-Kana, R. 1996, ApJ, 468, 17
Bar-Kana, R. 1997, ApJ, 489, 21
Beers, T. C., Flynn, K., & Gebhardt, K. 1990, AJ, 100, 32
Bertin, E., & Arnouts, S. 1996, A&AS, 117, 393
Blandford, R., Surpi, G., & Kundi'c, T. 2001, in Gravitational Lensing: Recent Progress and Future Goals (ASP Conference Proceedings, vol. 237), ed. T. G. Brainerd & C. S. Kochanek, p. 65
Browne, I. W. A., Wilkinson, P. N., Patnaik, A. R., & Wrobel, J. M. 1998, MNRAS, 293, 257
Bruzual, G., & Charlot, S. 1993, ApJ, 405, 538
Burud, I., et al. 2002, A&A, 383, 71
Carlberg, R. G., Yee, H. K. C., Morris, S. L., Lin, H., Hall, P. B., Patton, D. R., Sawicki, M., & Shepherd, C. W. 2001, ApJ, 552, 427
Chae, K.-H., Mao, S., & Augusto, P. 2001, MNRAS, 326, 1015
Chae, K. 2003, MNRAS, 346, 746
Chiba, M. 2002, ApJ, 565, 17
Cohn, J. D., Kochanek, C. S., McLeod, B. A., & Keeton, C. R. 2001, ApJ, 554, 1216
Cohn, J. D., & Kochanek, C. S. 2004, ApJ, 608, 25
Dalal, N., & Kochanek, C. S. 2002, ApJ, 572, 25
Dalal, N. & Watson, C. R. 2004, astro-ph/0409438
Danese, L., de Zotti, G., & di Tullio, G. 1980, A&A, 82, 322
Dobler, G., & Keeton, C. R. 2005, astro-ph/0502436
Fassnacht, C. D., & Lubin, L. M. 2002, AJ, 123, 627
Fassnacht, C. D., et al. 2004, Proceedings of IAU Symposium 225: Impact of Gravitational Lensing on Cosmology (also astro-ph/0409086)
Fassnacht, C. D., et al., astro-ph/0510728
Faure, C., Alloin, D., Kneib, J. P., & Courbin, F. 2004, A&A, 428, 741
Ferreras, I., Saha, P., & Williams, L. L. R. 2005, astro-ph/0503168
Fischer, P., Schade, D., & Barrientos, L. F. 1998, ApJ, 503, L127
Fukugita, M., Shimasaku, K., & Ichikawa, T. 1995, PASP, 107, 945
Gerke, B. F., et al. 2005, ApJ, 625, 6
Gorenstein, M. V., Shapiro, I. I., & Falco, E. E. 1988, ApJ, 327, 693
Grant, C. E., Bautz, M. W., Chartas, G., & Garmire, G. P. 2004, ApJ, 610, 686
Hege, E. K., Hubbard, E. N., Strittmatter, P. A., & Worden, S. P. 1981, ApJ, 248, L1
Henry, J. P., & Heasley, J. N. 1986, Nature, 321, 139
Hogg, D. W., & Blandford, R. D. 1994, MNRAS, 268, 889
Holder, G. P., & Schechter, P. L. 2003, ApJ, 589, 688
Impey, C. D., Foltz, C. B., Petry, C. E., Browne, I. W. A., & Patnaik, A. R. 1996, ApJ, 462, L53
Impey, C. D., Falco, E. E., Kochanek, C. S., Lehár, J., McLeod, B. A., Rix, H.-W., Peng, C. Y., & Keeton, C. R. 1998, ApJ, 509, 551
Keeton, C. R., Kochanek, C. S., & Seljak, U. 1997, ApJ, 482, 604
Keeton, C. R., & Kochanek, C. S. 1997, ApJ, 487, 42
Keeton, C. R., Kochanek, C. S., & Falco, E. E. 1998, ApJ, 509, 561
Keeton, C. R., Christlein, D., & Zabludoff, A. I. 2000, ApJ, 545, 129
Keeton, C. R. 2003, ApJ, 584, 664
Keeton, C. R., & Zabludoff, A. I. 2004, ApJ, 612, 660
Keeton, C. R., Gaudi, B. S., & Petters, A. O. 2005a, astro-ph/0503452
Keeton, C. R., et al., 2005b, in preparation
King, L. J., Browne, I. W. A., & Wilkinson, P. N. 1996, IAU Symp. 173: Astrophysical Applications of Gravitational Lensing, 173, 191
King, L. J., Browne, I. W. A., Marlow, D. R., Patnaik, A. R., & Wilkinson, P. N. 1999, MNRAS, 307, 225
Kneib, J., Cohen, J. G., & Hjorth, J. 2000, ApJ, 544, L35
Kochanek, C. S. 1991, ApJ, 373, 354
Kochanek, C. S. 1995, ApJ, 445, 559
Kochanek, C. S. 1996a, ApJ, 466, 638
Kochanek, C. S. 1996b, ApJ, 473, 595
Kochanek, C. S., et al. 2000, ApJ, 543, 131
Kochanek, C. S. & Schechter, P. L. 2003, in Measuring and Modeling the Universes (Carnegie Observatories Astrophysics Series, vol. 2), ed. W. L. Freedman (also astro-ph/0306040)
Kundić, T., Cohen, J. G., Blandford, R. D., & Lubin, L. M. 1997, AJ, 114, 507

Kundić, T., Hogg, D. W., Blandford, R. D., Cohen, J. G., Lubin, L. M., & Larkin, J. E. 1997, AJ, 114, 2276
Kurtz, M. J., & Mink, D. J. 1998, PASP, 110, 934
Langston, G. I., et al. 1988, BAAS, 20, 1001
Langston, G. I., et al. 1989, AJ, 97, 1283
Lehár, J., McMahon, R. G., Irwin, M. 1993, AAS, 183, 3307L
Lehár, J., et al. 1997, AJ, 114, 48L
Linder, E. V. 2004, Phys. Rev. D, 70, 043534
Lopez, S., Wucknitz, O., & Wisotzki, L. 1998, A&A, 339, L13
Mao, S., & Schneider, P. 1998, MNRAS, 295, 587
McMahon, R. & Irwin, M. 1992, Gemini, 36, 1M
Metcalf, R. B., & Madau, P.. 2001, ApJ, 563, 9
Mitchell, J. L., Keeton, C. R., Frieman, J. A, & Sheth, R. K. 2005, ApJ, 622, 81
Morgan, N. D., Kochanek, C. S., Pevunova, O. & Schechter, P. L. 2005, AJ, 129, 2531
Mulchaey, J. S. & Zabludoff, A. I. 1998, ApJ, 496, 73
Omont, A., McMahon, R. G., Cox, P., Kreysa, E., Bergeron, J., Pajot, F., & Storrie-Lombardi, L. J. 1996, A&A, 315, 1
Patnaik, A. R., Browne, I. W. A., Wilkinson, P. N., & Wrobel, J. M. 1992a, MNRAS, 254, 655
Patnaik, A. R., Browne, I. W. A., Walsh, D., Chaffee, F. H., & Foltz, C. B. 1992, MNRAS, 259, 1P
Postman, M., Lauer, T. R., Oegerle, W., & Donahue, M. 2002, ApJ, 579, 93
Premadi, P., & Martel, H. 2004, ApJ, 611, 1
Refsdal, S. 1964, MNRAS, 128, 307
Rusin, D., et al. 2001, ApJ, 557, 594
Rusin, D., & Tegmark, M. 2001, ApJ, 553, 709
Rusin, D., et al. 2003, ApJ, 587, 143
Rusin, D., & Kochanek, C. S. 2005, ApJ, 623, 666
Saha, P. 2000, AJ, 120, 1654
Schechter, P. L., et al. 1997, ApJ, 475, L85
Schneider, P., Ehlers, J., & Falco, E. E. 1992, Gravitational Lenses (Berlin: Springer)
Seljak, U. 1994, ApJ, 436, 509
Sheldon, E., et al. 2004, AJ, 127, 2544
Soucail, G., Kneib, J.-P., Jaunsen, A. O., Hjorth, J., Hattori, M., & Yamada, T. 2001, A&A, 367, 741
Tonry, J. L. 1998, AJ, 115, 1
Tonry, J. L., & Kochanek, C. S. 1999, AJ, 117, 2034
Tonry, J. L., & Kochanek, C. S. 2000, AJ, 119, 1078
Treu, T., & Koopmans, L. V. E. 2004, ApJ, 611, 739
Turner, E. L. 1990, ApJ, 365, L43
van Waerbeke, L., & Mellier, Y. 2003, astro-ph/0305089
Wambsganss, J., Bode, P., & Ostriker, J. P., 2004, astro-ph/0405147
Williams, K., Momcheva, I., Keeton, C. R., & Zabludoff, A. I. 2005, in preparation
Wilman, D. J., et al. 2005, astro-ph/0501183
Winn, J. N., Hall, P. B., & Schechter, P. L. 2003, ApJ, 597, 672
Winn, J. N., Hewitt, J. N., Patnaik, A. R., Schechter, P. L., Schommer, R. A., López, S., Maza, J., & Wachter, S. 2001, ApJ, 121, 122
Wisotzki, L., Köhler, T., Lopez, S., & Reimers, D. 1996, A&A, 315, L405
Weymann, R. J., et al. 1980, Nature, 285, 641
Wilkinson, P. N., Browne, I. W. A., Patnaik, A. R., Wrobel, J. M., & Sorathia, B. 1998, MNRAS, 300, 790
Yahil, A. & Vidal, N. V. 1977, ApJ, 214, 347
Young, P., Deverill, R. S., Gunn, J. E., Westphal, J. A., & Kristian, J. 1981, ApJ, 244, 723
Young, P., Gunn, J. E., Oke, J. B., Westphal, J. A., & Kristian, J. 1981, ApJ, 244, 736
Zabludoff, A. I., & Mulchaey, J. S. 1998, ApJ, 496, 39
Zabludoff, A. I., & Mulchaey, J. S. 1998, ApJ, 498, L5

APPENDIX

FORMALISM FOR CONVERGENCE AND SHEAR

Keeton (2003) presents a formalism for deriving a simple analytic estimates of the effective convergence $\kappa_{\rm eff}$ and shear $\gamma_{\rm eff}$ produced by a perturber somewhere along the line of sight to a lens. The same formalism can be used for all the situations considered in the main text (see §§4.4 and 4.5). The only assumption is that the convergence and shear are small, so that we can work at first order in both quantities. We will show below that there is a context in which this assumption breaks down, but with no effect on our conclusions.

If the perturber were at the same redshift as the lens galaxy, it would produce a convergence and shear given by

$$\kappa = \frac{1}{2}\left(\frac{\partial^2\varphi_{\rm pert}}{\partial x^2} + \frac{\partial^2\varphi_{\rm pert}}{\partial y^2}\right) , \tag{A1}$$

$$\gamma_c = \frac{1}{2}\left(\frac{\partial^2\varphi_{\rm pert}}{\partial x^2} - \frac{\partial^2\varphi_{\rm pert}}{\partial y^2}\right) , \tag{A2}$$

$$\gamma_s = \frac{\partial^2\varphi_{\rm pert}}{\partial x\,\partial y} , \tag{A3}$$

$$\gamma = \sqrt{\gamma_c^2 + \gamma_s^2} , \tag{A4}$$

$$\theta_\gamma = \frac{1}{2}\tan^{-1}\left(\frac{\gamma_s}{\gamma_c}\right) , \tag{A5}$$

where $\varphi_{\rm pert}$ is the lens potential of the perturber. Here γ is the shear strength, and θ_γ the shear direction (which we measure North through East). If the perturber lies at a different redshift $z_{\rm pert} \neq z_l$, then the convergence and shear are modified to the effective values (Keeton 2003)

$$\kappa_{\rm eff} = \frac{(1-\beta)\left[\kappa - \beta(\kappa^2 - \gamma^2)\right]}{(1-\beta\kappa)^2 - (\beta\gamma)^2} , \tag{A6}$$

$$\gamma_{\rm eff} = \frac{(1-\beta)\gamma}{(1-\beta\kappa)^2 - (\beta\gamma)^2} , \tag{A7}$$

where

$$\beta = \frac{D(z_1, z_2)}{D(0, z_2)}\,\frac{D(0, z_s)}{D(z_1, z_s)} , \tag{A8}$$

$$z_1 = \min(z_l, z_{\rm pert}) , \tag{A9}$$

$$z_2 = \max(z_l, z_{\rm pert}) , \tag{A10}$$

where $D(z_1, z_2)$ is the angular diameter distance between redshifts z_1 and z_2. Note that when $z_{\rm pert} = z_l$, we have $\beta = 0$ and so we recover $\kappa_{\rm eff} = \kappa$ and $\gamma_{\rm eff} = \gamma$. Moving the perturber away from the lens redshift increases β and decreases $\kappa_{\rm eff}$ and $\gamma_{\rm eff}$.

In certain circumstances, the effective convergence and shear can apparently go negative, which seems puzzling. The sign flip occurs only when the denominator in eqs. (A6)–(A7) goes negative. This can happen only when κ and γ are sufficiently large — in particular, only when the line of sight passes through the *strong lensing* regime of the perturber. (For an isothermal sphere [below], this corresponds to $\kappa, \gamma \geq 0.5$.) In this case, the lensing critical curves of the perturber would merge with those of the main lens galaxy, which would completely change the configuration of lensed images. In other words, our formalism breaks down when the "perturbation" is sufficiently strong, but if it were that strong it would (presumably) be known already.

If κ and γ are small, then we can expand eqs. (A6)–(A7) to first order write

$$\frac{\kappa_{\rm eff}}{\kappa} \approx \frac{\gamma_{\rm eff}}{\gamma} \approx 1 - \beta \,. \tag{A11}$$

We can think of $\kappa_{\rm eff}/\kappa$ and $\gamma_{\rm eff}/\gamma$ as the "normalized" convergence and shear — the actual perturbation strength, normalized by the value that would apply if the perturber were at the same redshift as the lens galaxy. We use this quantity in the text as a simple way to characterize the redshift dependence of the perturbation strength.

We now specify how to determine the net convergence and shear when multiple perturbers are present. This is relevant when we assess the effects of a group around a lens by considering the member galaxies (§4.4.2), and also when we consider the effects of structures along the line of sight (§4.5.2). We see from eqs. (A1)–(A3) that the quantities κ, γ_c, and γ_s are linear in the perturber potential. The shear is a combination of γ_c and γ_s that actually corresponds to a rank-2 traceless tensor, or a headless vector (headless because it is invariant under rotation by 180°). (See Schneider et al. 1992 for more discussion.) Thus, if we know the effective convergence $\kappa_{{\rm eff},i}$ and shear $\gamma_{{\rm eff},i}$, as well as the shear position angle $\theta_{\gamma,i}$ (North through East), for a set of perturbers, then the proper way to compute the net effects is as follows:

$$\kappa_{\rm tot} = \sum_i \kappa_{{\rm eff},i} \,. \tag{A12}$$

$$\gamma_{c,{\rm tot}} = \sum_i \gamma_{{\rm eff},i} \cos 2\theta_{\gamma,i} \,, \tag{A13}$$

$$\gamma_{s,{\rm tot}} = \sum_i \gamma_{{\rm eff},i} \sin 2\theta_{\gamma,i} \,, \tag{A14}$$

$$\gamma_{\rm tot} = \sqrt{\gamma_{c,{\rm tot}}^2 + \gamma_{s,{\rm tot}}^2} \,, \tag{A15}$$

$$\theta_{\gamma,{\rm tot}} = \frac{1}{2} \tan^{-1}(\gamma_{s,{\rm tot}}/\gamma_{c,{\rm tot}}) \,. \tag{A16}$$

Note that $\kappa_{{\rm eff},i} \geq 0$ for any real perturber, so the terms in the convergence sum all go in the same direction. By contrast, the cosine and sine factors mean that terms in the shear sums may add or cancel. Hence, incompleteness in our sample can only cause us to underestimate $\kappa_{\rm tot}$, but it may cause us to over- or underestimate $\gamma_{\rm tot}$.

It is worthwhile to recall how convergence and shear affect lens models. Convergence is largely responsible for systematic biases in lens models (KZ04), through the mass sheet degeneracy (Gorenstein et al. 1988; Saha 2000). The biases can be thought of as simple rescalings of model parameters, such as:

$$\beta \propto (1 - \kappa_{\rm tot}) \,, \tag{A17}$$

$$h \propto (1 - \kappa_{\rm tot}) \,, \tag{A18}$$

$$\mu \propto (1 - \kappa_{\rm tot})^{-2} \,, \tag{A19}$$

where β is a mass parameter related to the lens velocity dispersion, h is the Hubble parameter, and μ is the image magnification (see KZ04 and references therein). Neglect of convergence is the main source of biases in lensing results for quad lenses. Double lenses, by contrast, are so under-constrained that poor knowledge of convergence and shear leads to lens models that are just plain wrong. In both cases, detailed observations of lens environments are necessary to derive the constraints necessary to make lens models reliable.

While the formalism presented so far is fully general, it is valuable to discuss two particular perturber models. First, if we can approximate a perturber as an isothermal sphere then we can easily relate measurable quantities to κ and γ. Specifically, for an isothermal sphere with velocity dispersion σ and impact parameter b, we have

$$\kappa = \gamma = 1.44 \times 10^{-5} \left(\frac{1''}{b}\right) \left(\frac{\sigma}{\rm km/s}\right)^2 \frac{D(z_{\rm pert}, z_s)}{D(0, z_s)} \,. \tag{A20}$$

We can measure the line-of-sight velocity dispersion σ_r of the group and the offset b between the lens galaxy and group centroid, use them to determine κ and γ, and finally fold in the redshift difference as above to determine $\kappa_{\rm eff}$ and $\gamma_{\rm eff}$.

The second specific model we consider is a power law density profile calibrated by weak lensing. In a large and detailed analysis of galaxy–galaxy weak lensing in the Sloan Digital Sky Survey, Sheldon et al. (2005) present the

average shear as a function of radius for a sample of 127,001 lens galaxies. They find that the shear profile is consistent with a simple power law

$$\gamma(R) = \frac{A}{\Sigma_{\rm crit}}\ R^{-\alpha}\,, \tag{A21}$$

where $\Sigma_{\rm crit} = (c^2 D_{os})/(4\pi G D_{ol} D_{ls})$ is the critical surface density for lensing, which carries all the dependence on the lens and source redshifts through the angular diameter distances D_{ol}, D_{os}, and D_{ls} between the observer, lens, and source. Sheldon et al. tabulate the values of α and A for galaxies in three luminosity bins.[6] For any given galaxy that we observe, we convert from our measured I-band apparent magnitude to absolute magnitude in the SDSS i-band, using the color and K-corrections computed with Bruzual & Charlot (1993) spectral synthesis models. (The luminosity bins used by Sheldon et al. are wide enough that small systematic uncertainties in the magnitudes do not shift galaxies between bins.) We then look up the values of A and α for each luminosity from Table 2 of Sheldon et al. We use the lens and source redshifts to compute $\Sigma_{\rm crit}$ and hence $\gamma(R)$. The last thing we need is the convergence. For a power law $\gamma(R) \propto R^{-\alpha}$, there is a very simple relation between shear and convergence:

$$\kappa(R) = \frac{2-\alpha}{\alpha}\ \gamma(R)\,. \tag{A22}$$

Thus, it is straightforward to compute κ and γ for each galaxy. We can then factor in the redshift distance relative to the main lens galaxy as described above.

[6] Sheldon et al. (2005) actually tabulate power law parameters for the galaxy–mass correlation function rather than the shear directly, but their formalism makes it straightforward to convert back to A and α. At any rate, those parameters are more fundamental in terms of what they measure. One additional technical point is that Sheldon et al. quote lengths using comoving distances, but we convert those to angular diameter distances in our analysis.

This figure "f6_sm.jpg" is available in "jpg" format from:

http://arXiv.org/ps/astro-ph/0511594v1